Research Square

Preprints are preliminary reports that have not undergone peer review. They should not be considered conclusive, used to inform clinical practice, or referenced by the media as validated information.

One-dimensional heterogeneity variography for critical point identification in environmental monitoring: a methodology based on Gy's sampling theory

Christian Romero Prieto

c.romero@nostertec.com

Noster Tec SRL

Research Article

Keywords: heterogeneity variography, critical point identification, river sediment contamination, Value for Critical Comparisons, Gy sampling theory, environmental monitoring

Posted Date: September 28th, 2026

DOI: https://doi.org/10.21203/rs.3.rs-10177583/v1

License: This work is licensed under a Creative Commons Attribution 4.0 International License. Read Full License

Additional Declarations: No competing interests reported.

One-dimensional heterogeneity variography for critical point identification in environmental monitoring: a methodology based on Gy's sampling theory

Christian Romero Prieto [1]

1 Noster Tec SRL, La Paz – Bolivia; c.romero@nostertec.com

Abstract

This study introduces a methodology for identifying critical sampling points in river systems, grounded in the one-dimensional heterogeneity variography formalized by Pierre Gy within sampling theory, unlike the multidimensional Matheron geostatistical variogram. This approach operates on sequentially ordered sampling series such as river transects, where a one-dimensional model is both theoretically justified and operationally sufficient for datasets of six or more stations.

The central contribution is the Value for Critical Comparisons (VCC_{Norm}), an adaptive threshold derived empirically from the statistical structure of each composite normalized variogram. The VCC_{Norm} scales automatically with the magnitude and dispersion of the dataset, enabling objective identification of sampling points whose normalized variance exceeds the system's characteristic variability and without reference to external regulatory standards. This makes the methodology applicable in data-scarce or regulation-deficient contexts where conventional pollution indices may be unavailable or contested.

Efficacy is validated through four independent case studies of contaminated rivers in Asia, Europe, and South America: the Tamla Nala stream (Durgapur, India), the Warta River (Poland), the Elbe River (Germany), and the Orckojahuira River (La Paz, Bolivia). In all cases, VCC_{Norm}-based critical point identification is consistent with conclusions reached by the original investigators using pollution indices, enrichment factors, cluster analysis, and direct field observation. The VCC_{Norm}values across all datasets fall within a narrow range (≈0.15–0.22), confirming the adaptive and consistent behavior of the empirical estimator. Positioned as a complementary tool to existing environmental quality frameworks, the methodology provides individual station-level spatial resolution that complements the group-level characterization offered by cluster analysis. A VBA-Excel™ application named TruVariogram has been developed to streamline implementation.

Keywords: *heterogeneity variography; critical point identification; river sediment contamination; Value for Critical Comparisons; Gy sampling theory; environmental monitoring*

Introduction

Variography is a statistical method for characterizing spatial and temporal variability in sequentially ordered datasets. Its most widely recognized form, the Matheron geostatistical variogram (Matheron, 1965), describes the spatial correlation structure of regionalized variables across continuous two- or three-dimensional fields and underpins interpolation methods such as kriging (Webster & Oliver, 2007). A distinct but related framework (Minnitt & Esbensen, 2017), developed by Pierre Gy within the theory of sampling (Gy, 1992b), applies variography to one-dimensional ordered series —such as discrete sampling stations arranged along a river, a geological borehole, or a temporal monitoring sequence— to characterize heterogeneity and variability along a single axis. These two frameworks share foundational principles (stationarity, isotropy, ergodicity) but differ in dimensionality, computational structure, and intended application. The methodology presented in this study is grounded in Gy's one-dimensional framework.

Sampling stations are typically arranged in a defined linear order along a watercourse, and the primary objective is to detect critical points of elevated concentration along that axis —not to interpolate values across a continuous surface. A one-dimensional variographic model is both theoretically appropriate and operationally practical for this purpose. It requires no spatial interpolation, can be applied to the small datasets ($n \geq 6$) typical of field campaigns, and does not depend on fitted theoretical variogram models or on external regulatory thresholds.

The spatial distribution of analytes in fluvial systems is inherently stochastic, governed by factors that cannot be fully established or controlled —tectonic history, erosion, temperature cycles, biological activity, and the cumulative effects of anthropogenic pressure over extended timescales. Short-term events can equally reshape contamination patterns in hours or weeks. A dam breach, for instance, introduces tailings into a water body (Hoang et al., 2017) under the combined influence of discharge density, viscosity, pH, particle size, concentration fronts, and rupture pressure— each factor independently variable and collectively determining how contaminants

distribute through the system. Uncontrolled industrial or urban effluent discharges present analogous complexity, where the formation, dissolution, and redistribution of pollutants in sediments depend on a similarly large set of interacting variables.

The stochastic character of these anthropogenically induced events is compounded by the dynamic behavior of sediments themselves. Hydrodynamic forces during flood events can mobilize and redistribute contaminated sediment across significant distances, fundamentally altering spatial concentration patterns in ways that may not be captured by pre-event monitoring data (Gordon et al., 2007). Beyond transport, sediments act as both sources and sinks of dissolved contaminants: depending on pH, redox potential, ion incorporation, and the presence of complexing agents, the same sediment may release or sequester pollutants over time (Arze Landivar et al., 2025). This dual role makes sediment monitoring a particularly demanding analytical challenge, and one where the identification of spatially anomalous points —rather than system-wide averages— is of direct practical value.

Recent advances in geostatistics have strengthened environmental impact assessment (EIA) and strategic environmental assessment (SEA) through improved tools for modeling spatial variability in pollution and risk contexts (Alshahrani et al., 2025; Mayer, 2025). However, these approaches typically require substantial datasets, fitted theoretical models, and may rely on predefined regulatory indices —such as the Toxic Equivalent Quotient (TEQ), Pollution Load Index (PLI), or Geoaccumulation Index (Igeo)— that may not exist for all parameters or regions of interest (Fortuna et al., 2022; Onyango et al., 2021). Traditional statistical summaries —means, ranges, cluster analysis— characterize contamination patterns globally but may fail to pinpoint the specific sampling locations responsible for the observed variation, limiting their utility for targeted remediation and adaptive monitoring design. Variography provide more accurate characterizations of spatial variation compared to classical statistical methods (de Alves et al., 2011).

To address these limitations, this study introduces a methodology based on one-dimensional heterogeneity variography and a normalized threshold parameter termed the Value for Critical Comparisons (VCC_{Norm}). The VCC_{Norm} is derived from the statistical structure of the variogram itself, enabling objective identification of sampling points whose associated normalized variance exceeds the characteristic variability of the system, i.e. without reference to external regulatory standards. This makes the approach applicable in contexts where established benchmarks are absent, incomplete, or contested, and serves as a data-driven complement to existing assessment frameworks.

The methodology is validated through four independent case studies: the Tamla Nala stream (Durgapur, India), the Warta River (Poland), the Elbe River (Germany), and the Orckojahuira River (La Paz, Bolivia). In each case, results are compared against independent conclusions from the original investigators, who employed pollution indices, enrichment factors, cluster analysis, and direct field observation. To support practical implementation, a VBA-Excel™ application named TruVariogram has been developed, streamlining variogram construction and VCC evaluation for environmental practitioners.

Variographic framework: heterogeneity and the experimental variogram

The variographic formulation employed in this study follows the one-dimensional heterogeneity framework developed by Pierre Gy (Gy, 1992b), in which a set of environmental sampling stations arranged in a defined linear sequence —along a river, a geological borehole, or a temporal monitoring axis— is treated as an ordered series of discrete units. This approach is distinct from the classical Matheron geostatistical variogram (Matheron, 1965) used in kriging applications, which characterizes the spatial correlation structure of a regionalized variable across a continuous multidimensional field. Gy's one-dimensional framework is the appropriate choice when the ordering of sampling units along a single axis is the primary spatial dimension of interest, and when the objective is to identify points of anomalous variability along that axis rather than to interpolate values across a surface.

The theoretical foundations of this framework rest on three statistical principles (Webster & Oliver, 2007):

- **Stationarity** implies that the statistical properties of the process —mean and variance— remain constant regardless of the position along the sampling axis. For example, if analyte concentrations in a river are stationary, their average and spread do not systematically increase or decrease from upstream to downstream.
- **Isotropy** assumes that these properties are uniform in all directions. In the one-dimensional context of this study, isotropy holds along the single sampling axis by construction, since stations are regularly spaced and the variogram is computed along that axis only.
- **Ergodicity** adds that observations from a sufficiently long sequence are representative of the statistical behavior of the entire system, allowing the spatial variogram to be estimated from a single realization of the process.

In practice, environmental data frequently depart from strict stationarity. This necessitates the use of heterogeneity-normalized variables (see Equation 4) rather than raw concentrations, which both stabilizes the variance and enables comparison across parameters with different units and magnitudes.

Stationarity and semivariance

In an ideally homogeneous system, the property h at any sampling point q would equal that at any other point $q + j$, and the expected squared difference between them would be zero:

$$E\left(h_q - h_{q+j}\right)^2 = 0 \qquad 1$$

In real systems, stochastic variability introduces deviations from this ideal. Georges Matheron (Matheron, 1965) proposed capturing this residual variability through the semivariance —half the mean squared difference between pairs of observations. In the one-dimensional ordered-series context of Gy's framework (Gy, 1992a), the semivariance at *lag j* is expressed as:

$$Var\left(h_q - h_{q+j}\right) = v(j) = \frac{1}{2N_U}\sum_q \left(h_q - h_{q+j}\right)^2 \qquad 2$$

For a finite ordered series with N_U sampling units, and accounting for the decreasing number of available pairs as the lag increases, the experimental variogram is formalized as:

$$v(j) = \frac{1}{2(N_U - j)}\sum_q \left(h_q - h_{q+j}\right)^2 \qquad 3$$

Definition of *lag* in the one-dimensional ordered-series context

In the one-dimensional sequential variography employed here, the term *lag j* denotes the integer step separating two sampling units in the ordered series. For a regularly spaced sampling campaign in which stations are separated by a uniform interval Δ, lag $j = 1$ corresponds to pairs separated by Δ, lag $j = 2$ to pairs separated by 2Δ, and so on. This definition differs from the lag concept used in the classical Matheron variogram, where lag h is a distance vector —or scalar tolerance band— that groups all pairs of observations separated by approximately that distance across a continuous spatial field, regardless of their sequential position. In the one-dimensional ordered-series formulation used here, lag j indexes the step size within the sequence, and for each lag, all pairs $(q, q + j)$ with $q = 1$ to $N_U - j$ are included in the calculation. The number of available pairs therefore equals $N_U - j$ and decreases as j increases. To illustrate, for a river with eight sampling stations and lag $j = 2$, the pairs included in the calculation of $v(2)$ are (1,3), (2,4), (3,5), (4,6), (5,7), and (6,8), i.e. a total of six pairs. This is consistent with standard geostatistical practice of using all available pairs at a given lag, adapted to the one-dimensional ordered-series context.

Heterogeneity normalization

Equation 3 can in principle be applied to any measured property. However, analyte concentrations are neither additive nor subtractive unless they refer to the same volume or mass (Arze Landivar et al., 2025), and direct application to concentrations yields variance values with units of concentration squared, making cross-parameter comparison impossible. To address this, the property h_q in Equation 3 is defined as the relative heterogeneity of sample q, following Gy (Gy, 1992a):

$$h_q = \frac{a_q - a_L}{a_L} \cdot \frac{m_q \cdot N_U}{m_L} \qquad 4$$

Where a_L is the weighted mean concentration across all samples, defined as:

$$a_L = \frac{1}{m_L}\sum_q a_q \cdot m_q \qquad 5$$

and m_q, m_L, and N_U are the sample mass, total batch mass, and number of sampling units, respectively. Note that a_L differs from the simple arithmetic mean when sample masses are unequal. By substituting h_q for raw concentration

in Equation 3, the resulting variogram values $v(j)$ are dimensionless and directly comparable across parameters regardless of their original units or magnitudes.

Pierre Gy extended this framework to three types of batches that can all be modeled as one-dimensional ordered series (Gy, 1992b), i.e. ordered discrete units (U_q), such as sequential river sediment samples; continuous stationary particulate solids, such as sediment deposited in a lentic system; and continuous moving flows, such as fluvial systems or fixed-station temporal monitoring at regular intervals. In all three cases, the variogram in Equation 3 applied to the heterogeneity of Equation 4 provides a unified characterization of variability along the one-dimensional ordering axis.

Components of the experimental variogram

The experimental variogram defined by Equations 3 and 4 is characterized by three structural components:

- **Nugget, $\boldsymbol{v(0)}$**: the variogram value extrapolated to lag zero, representing variability at distances shorter than the minimum sampling interval —attributable to measurement error, sub-sampling heterogeneity, or natural micro-scale variability. Since no pairs exist at distance zero, $v(0)$ is estimated by fitting a fifth-degree polynomial to $v(1)$ through $v(5)$ and reading the intercept. If the intercept is negative, $v(0) = 0$ is assigned.
- **Sill**: the maximum variogram value observed across all lags, indicating that beyond a certain separation distance, semivariance no longer increases and spatial autocorrelation is lost. In the one-dimensional ordered-series context, the sill is the highest $v(j)$ value observed within the available dataset —not an asymptotic theoretical plateau as in fitted geostatistical models.
- **Range**: the lag distance at which the variogram reaches the sill. Points separated by fewer lags than the range exhibit spatial correlation; those beyond the range are treated as independent.

These components inform the interpretation of the variogram and the selection of the VCC_{Norm}threshold described in the following subsection.

$\boldsymbol{VCC}$ methodology for critical point identification

The algorithmic logic for identifying critical points is depicted in Figure 1. The procedure integrates the heterogeneity variogram described in the preceding subsection with the normalized threshold parameter VCC_{Norm} and a set of optional complementary criteria. A sampling point $q$is flagged as critical when the following inequality holds:

$$v(j)_{Norm} > VCC_{Norm} \tag{6}$$

where $v(j)_{Norm}$is the normalized heterogeneity semivariance at lag j (Equation 8), associated with sampling point $q$through the relationship $v(q) = v(j-1)$ (Equation 14). Unlike fixed regulatory thresholds —which depend on external standards such as the PLI or the TEQ— the VCC_{Norm} is derived from the statistical structure of the variogram itself, making it intrinsically scaled to the magnitude and dispersion of each dataset.

Empirical estimation of the $\boldsymbol{VCC_{Norm}}$

Raw heterogeneity variances $v(j)$are first normalized (Equation 8) to produce $v(j)_{Norm}$, which has mean $\approx 0$and standard deviation $\approx 1$by construction, enabling direct comparison across parameters with different units or magnitudes. The $VCC_{Norm}$is then estimated directly from the normalized variogram data using the following empirical estimator:

$$VCC_{Norm} = \sqrt{\frac{\sum_{j=0}^{N_U} v(j)_{norm}{}^2}{v_{Norm,max} - v_{Norm,min}}} \cdot \frac{s_{v_{Norm}}}{10} \tag{7}$$

where $v_{Norm,max}$ and $v_{Norm,min}$ are the maximum and minimum values of $v(j)_{Norm}$, and $s_{v_{Norm}}$ is the sample standard deviation of the $v(j)_{Norm}$values.

Note that Equation 7 may also be applied directly to raw heterogeneity variances $v(j)$ to obtain a parameter-specific VCC for single-parameter variograms. In that case, v_{max}, v_{min}, and s_v refer to the raw $v(j)$ values, and the resulting VCC carries the same units as $v(j)$. All case studies in this work employ the normalized form (VCC_{Norm}) to enable multi-parameter composite evaluation.

The estimator combines two components. The first, $\sqrt{\sum_{j=0}^{N_U} v(j)_{Norm}^2 \,/\, (v_{Norm,max} - v_{Norm,min})}$, is the root-mean-square (RMS) of the normalized variogram values scaled by the observed amplitude of variation. The second, $s_{v_{Norm}}/10$, scales the result to the typical magnitude of $v(j)_{Norm}$ distributions observed in environmental monitoring datasets. Their product gives VCC_{Norm} a self-regulating character: in homogeneous systems with a flat variogram, both components are small, yielding a low threshold; in heterogeneous systems with a strongly rising variogram, both are proportionally larger. The VCC_{Norm} thereby adapts automatically to the scale of variability of each dataset.

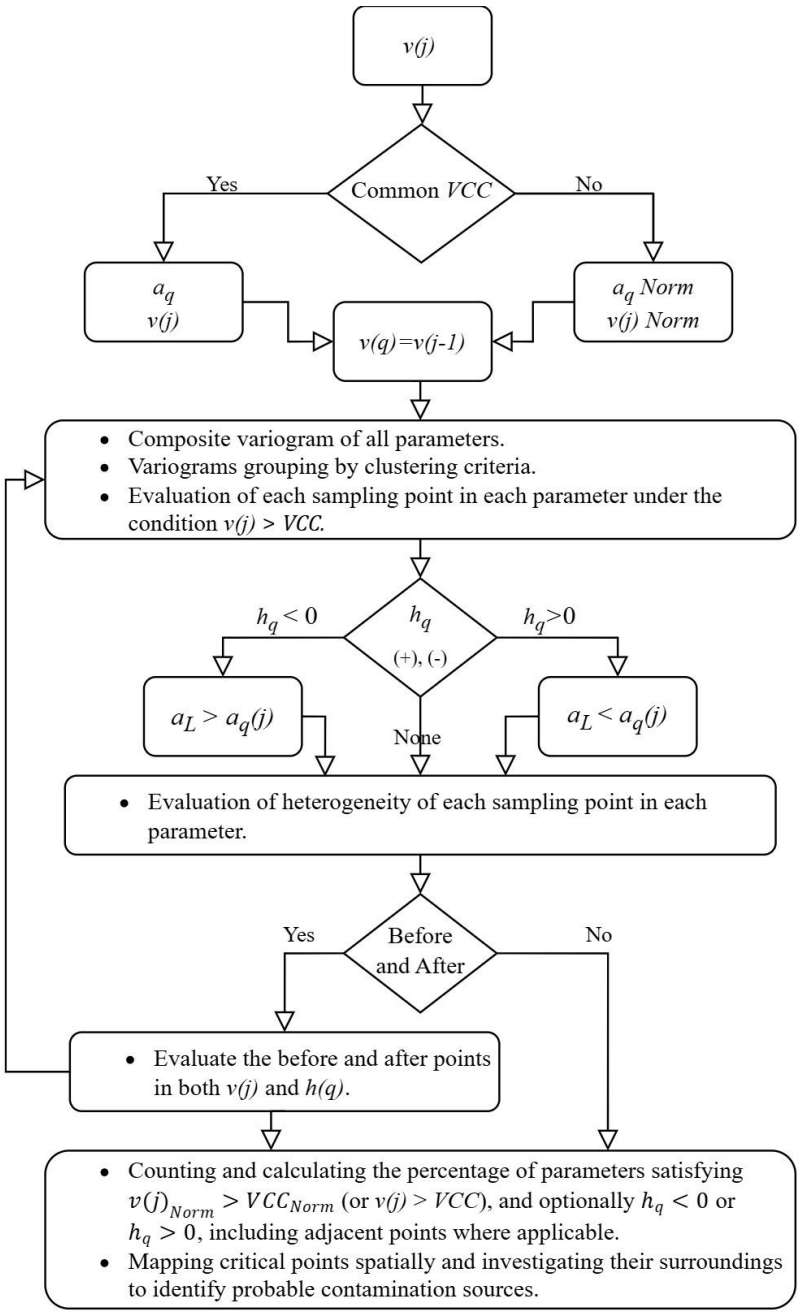

Figure 1. Flowchart depicting the algorithmic logic for identifying critical sampling points using one-dimensional heterogeneity variography and the VCC_{Norm} criterion (Eq. 6), with optional complementary evaluation based on heterogeneity sign h_q(Eq. 12) and adjacent point assessment (Eq. 13).

Symbols: Rectangles represent processes; diamonds indicate decisions; arrows show flow.

Source: Author's own elaboration

This estimator has been verified against all four case studies. Applied parameter by parameter and averaged over all parameters in each composite variogram, Equation 7 reproduces the VCC_{Norm} values used in the analyses to within 0.1–8% across all datasets (Table 9). This correspondence confirms that Equation 7 is not an approximation introduced post-hoc but the underlying quantitative basis for the thresholds applied throughout this study.

A sampling point is flagged as critical when $v(j)_{Norm} > VCC_{Norm}$ (Equation 6), which is equivalent to identifying points whose normalized variance exceeds VCC_{Norm} standard deviations above the variogram mean. The value of VCC_{Norm} controls the trade-off between sensitivity and specificity as it is detailed in Table 1.

Table 1. VCC_{Norm} values, their statistical interpretation, and recommended use in environmental monitoring.

VCC_{Norm}	Approx. % flagged	Recommended use
0.15	~35%	Good sensitivity
0.20	~32%	Exploratory screening
0.25	~27%	General environmental monitoring
0.50	~23%	Standard assessment
1.00	~12%	Conservative screening

The VCC_{Norm} functions as a sensitivity parameter analogous to a significance level in statistical hypothesis testing: it does not define contamination *per se* but identifies the threshold above which a sampling point warrants further investigation.

Complementary evaluation criteria

In addition to the primary criterion (Equation 6), the following criteria may be applied to further characterize critical points (Figure 1):

Normalized variance:

$$v(j)_{Norm} = \frac{v(j) - \overline{v}}{s_v} \quad (8)$$

where, $\overline{v}$, is the average variance of the variogram, and s_v is the standard deviation of the variogram.

Normalized concentration:

$$a_{q_{Norm}} = \frac{a_q - a_L}{s_a} \quad (9)$$

where, s_a is the standard deviation of the concentrations.

Normalized heterogeneity:

$$h_{q_{Norm}} = \frac{a_{q_{Norm}} - a_L}{a_L} \cdot \frac{m_{q_{Norm}} \cdot N_U}{m_L} \quad (10)$$

where, $m_{q_{Norm}}$ is the normalized mass (see the following equation).

Normalized mass:

$$m_{q_{Norm}} = \frac{m_q - m_L}{s_m} \quad (11)$$

where, m_q is the mass of the sample at point q, m_L is the mass of the batch, and s_m is the standard deviation of the masses.

Positive or negative heterogeneity value:

$$h_q < 0, h_q > 0 \quad (12)$$

where, if these inequalities hold independently, the sampling point corresponding to $v(j)$ must be evaluated.

Evaluation of variance before and after:

$$v(j)_{Norm} > VCC_{Norm} \quad (13)$$

when this inequality holds for a given lag j, the immediately adjacent points $v(j-1)$, $v(j)$, and $v(j+1)$, are also flagged for evaluation to detect gradients associated with localized point sources.

The four combinations of variogram type resulting from these criteria are summarized in Table 2.

Table 2. Combinations of experimental and normalized variograms.

	a_q	$a_{q_{Norm}}$
$v(j)$	Variogram	Variogram with normalized concentration
$v(j)_{Norm}$	Variogram with normalized variance	Variogram with normalized concentration and variance

Assignment of variance to sampling points

Once $v(j)$ values are obtained for all lags j, including $v(0)$, estimated by fifth-degree polynomial regression through $v(1)$ to $v(5)$ [1] (Teegavarapu, 2007) —sampling points are overlaid onto the variogram. Point $q = 1$ corresponds to $v(0)$; point $q = 2$ to $v(1)$; and so on. The general relationship is established in Equation 14. Critical sampling points are highlighted in red on both individual and composite variograms.

$$v(q) = v(j-1) \tag{14}$$

Manual intervention and field validation

The methodology permits manual intervention to define critical points based on professional judgment derived from field observations —including discolored sediments, characteristic odors, or proximity to discharge points— when visual evidence provides direct information not captured by the statistical criteria. Critical points are subsequently investigated in relation to geographic information (satellite imagery, field data) to identify probable contamination sources.

VCC_{Norm} as a complement to EIA/SEA

The VCC_{Norm} operates as a complementary analytical tool within Environmental Impact Assessment (EIA) and Strategic Environmental Assessment (SEA) frameworks. Unlike regulatory indices —such as the TEQ or PLI— that require comparison against predefined standards, the VCC_{Norm} is derived from the variogram's own statistical structure and is therefore applicable in contexts where established benchmarks are absent, incomplete, or contested. Its outputs are advisory: the methodology identifies sampling points warranting further investigation, rather than establishing legal compliance or exceedance of regulatory thresholds. In the four case studies presented, it consistently identified the same critical points as those determined by the original investigators using independent methodologies, while providing spatial resolution at the individual station level that complement the group-level characterization offered by cluster analysis and global pollution indices.

Selection of case studies

Scientific publications reporting tabulated analyte concentration data with referenced sampling locations were identified for methodology testing. Selection criteria required: (1) sufficient data for variogram calculation at a minimum of six sequential stations; (2) explicit geographic referencing of sampling locations; and (3) independent conclusions by the original authors against which VCC_{Norm}-based results could be compared. The four case studies satisfying these criteria —Tamla Nala (India), Warta (Poland), Elbe (Germany), and Orckojahuira (Bolivia)— are described in the following section. To avoid overloading the main text, some tables and graphs have been included in the supplementary material of this article.

[1] The intercept of the polynomial (independent term a) corresponds to $v(0)$ when $j = 0$. Since a negative variance has no physical interpretation, if $a < 0$ then $v(0) = 0$ is assigned.

1. **K. K. Pobi et al. in 2019: "Sources evaluation and ecological risk assessment of heavy metals accumulated within a natural stream of Durgapur industrial zone, India, by using multivariate analysis and pollution indices".**

The publication by Krishnendu Kumar Pobi and his team (Pobi et al., 2019) analyzes variations in physicochemical parameters and heavy metal contamination in the water and sediments of the Tamla Nala natural stream, located in the Durgapur industrial zone, India. The results indicate that pH values, chemical oxygen demand, chloride ions, cyanide, and concentrations of heavy metals such as lead, mercury, and iron in the water samples exceed the standards set by Indian regulations. Using pollution indices and multivariate analysis, the authors conclude that the presence of heavy metals in water and sediments is primarily due to industrial discharges.

The study provides detailed measurement data for water samples but does not include equivalent information for sediments. For this reason, the variography evaluation is limited to surface water samples. The parameters analyzed by K. K. Pobi et al. in water samples include: pH, temperature, electrical conductivity (EC), total dissolved solids (TDS), total hardness (TH), biological oxygen demand (BOD), chemical oxygen demand (COD), nitrate (NO_3^-), phosphate (PO_4^{3-}), sulfate (SO_4^{2-}), chloride (Cl^-), cyanide (CN^-), sodium (Na), potassium (K), lead (Pb), cadmium (Cd), chromium (Cr), iron (Fe), copper (Cu), nickel (Ni), and mercury (Hg).

The parameters were classified into two groups based on their variograms: (i) BOD, COD, and anions (NO_3^-, PO_4^{3-}, SO_4^{2-}, Cl^-, CN^-); and (ii) cations (Na, K, Pb, Cd, Cr, Fe, Cu, Ni, Hg). A normalized VCC_{Norm} of 0.158 was applied to the anion group and 0.154 to the cation group, both derived from the empirical estimator (Equation 7) applied to the corresponding composite variograms. No heterogeneity criteria were applied, nor was an explicit identification of concentrations before and after detected critical points conducted.

Of the 128 parameter-point combinations evaluated (16 parameters × 8 sampling points), 52 were identified as critical, corresponding to 40.6%. The spatial distribution of critical parameters exhibits a clear downstream intensification pattern consistent with the location of industrial facilities along the watercourse. Sampling point S1, located upstream of any documented industrial influence, presents no critical parameters under either group, confirming its role as a baseline reference. From S2 onward, critical parameters emerge progressively: S2 flags NO_3^- alone; S3 adds COD, Cl^-, and Hg; by S5, nine parameters are critical including CN^-, Pb, Cd, and multiple heavy metals; and S6 reaches 14 critical parameters (87.5% of all evaluated), coinciding spatially with the highest density of industrial facilities —two chemical plants and one pharmaceutical plant— identified in the vicinity through Google Earth imagery. The detailed results of these calculations are presented in Table 3 and Figure 2.

Table 3. Calculated normalized variance values $v(j)_{Norm}$ and heterogeneity indices $h(q)$ based on parameters $a(q)$ reported by Pobi et al. (2019) for the Tamla Nala stream, Durgapur industrial zone, India. A VCC_{Norm} of 0.158 was applied to the anion/BOD/COD group and 0.154 to the cation group. The evaluation comprises 128 parameter-point combinations (16 parameters × 8 sampling points).

Minigraph																	
v(q)/h(q)/a(q)		v(q)	h(q)	a(q)	v(q)	h(q)	a(q)	v(q)	h(q)	a(q)	v(q)	h(q)	a(q)	v(q)	h(q)	a(q)
Sample	**Distance**	**BOD**			**COD**			**NO_3^-**			**PO_4^{3-}**			**SO_4^{2-}**		
S1	1	-1.14E+00	-9.08E+02	26.41	-1.21E+00	-4.93E+02	423.59	-1.49E+00	3.40E+02	4.12	-1.28E+00	1.32E+03	0.57	-1.05E+00	7.91E+02	64.24
S2	2	-2.76E-01	-1.28E+03	26.19	-4.97E-02	-7.78E+02	417.63	6.56E-01	-1.18E+02	3.97	-1.12E+00	1.45E+03	0.55	-9.73E-01	4.07E+02	61.58
S3	3	-1.78E-02	7.00E+02	27.36	1.15E+00	1.58E+03	466.80	1.50E+00	6.73E+02	4.23	-6.46E-01	1.06E+03	0.60	-7.64E-01	7.82E+02	64.17
S4	4	-6.28E-01	6.35E+00	26.95	7.95E-01	1.33E+03	461.60	1.44E-01	-4.20E+01	4.00	-1.71E-01	1.26E+03	0.58	-4.01E-01	5.26E+02	62.41
S5	5	-3.86E-01	-3.15E+02	26.76	6.94E-01	-1.38E+02	431.00	-1.65E-01	-9.93E+02	3.68	7.45E-02	1.41E+03	0.56	1.01E-01	6.88E+00	58.81
S6	6	1.48E+00	5.14E+02	27.25	8.16E-01	-4.69E+02	424.10	7.05E-01	-2.81E+02	3.92	6.02E-01	-7.77E+02	0.83	5.30E-01	-4.39E+02	55.72
S7	7	1.59E+00	1.33E+03	27.73	-1.14E+00	-1.41E+02	430.94	-1.25E+00	7.85E+02	4.27	1.39E+00	-2.99E+03	1.11	7.12E-01	-7.76E+02	53.39
S8	8	-6.14E-01	-4.44E+01	26.92	-1.06E+00	-8.84E+02	415.42	-1.08E-01	-3.63E+02	3.89	1.16E+00	-2.73E+03	1.08	1.85E+00	-1.30E+03	49.77

Minigraph							
v(q)/h(q)/a(q)		v(q)	h(q)	a(q)	v(q)	h(q)	a(q)
Sample	**Distance**	**Cl^-**			**CN^-**		
S1	1	-1.91E+00	-1.62E+03	821.30	-7.75E-01	8.74E+03	0.70
S2	2	-7.06E-01	-2.15E+03	764.70	-8.18E-01	-1.22E+04	1.48
S3	3	2.40E-01	1.41E+03	1144.20	-5.86E-01	-8.65E+03	1.35
S4	4	2.79E-02	9.14E+02	1091.50	-3.87E-02	-6.45E+03	1.26
S5	5	-1.12E-01	4.89E+02	1046.10	5.47E-01	-4.36E+03	1.19
S6	6	6.84E-01	2.04E+02	1015.70	1.00E+00	1.45E+03	0.97
S7	7	1.49E+00	5.25E+02	1050.00	1.72E+00	5.07E+03	0.83
S8	8	2.82E-01	2.26E+02	1018.10	-1.06E+00	1.64E+04	0.41

Global: 56	22
	39.3%
A: Param.	**B: Cnt.**	**C: %**
NO_3^-	1	14.30%
COD, NO_3^-, Cl^-	3	42.90%
COD	1	14.30%
COD, CN^-	2	28.60%
BOD, COD, NO_3^-, PO_4^{3-}, SO_4^{2-}, Cl^-, CN^-	7	100.00%
BOD, PO_4^{3-}, SO_4^{2-}, Cl^-, CN^-	5	71.40%
PO_4^{3-}, SO_4^{2-}, Cl^-	3	42.90%

Table 3 Continuation

Sample	Distance	Na v(q)	Na h(q)	Na a(q)	K v(q)	K h(q)	K a(q)	Pb v(q)	Pb h(q)	Pb a(q)	Cd v(q)	Cd h(q)	Cd a(q)	Cr v(q)	Cr h(q)	Cr a(q)
S1	1	-1.05E+00	-8.54E+02	323.50	-1.39E+00	-3.61E+02	72.18	-1.21E+00	6.24E+02	2.80	-1.10E+00	3.99E+02	0.33	-9.92E-01	1.66E+03	0.55
S2	2	-8.20E-01	2.32E+02	348.70	-9.23E-01	3.34E+02	77.93	-1.00E+00	6.00E+01	2.53	-1.06E+00	-9.20E+01	0.31	-9.31E-01	1.13E+03	0.52
S3	3	-1.17E-01	1.22E+03	371.70	-3.89E-01	1.07E+03	83.99	-7.12E-01	9.16E+02	2.94	-7.35E-01	8.35E+02	0.35	-7.50E-01	5.71E+02	0.49
S4	4	5.82E-01	7.58E+02	360.90	-7.12E-02	5.99E+02	80.12	-2.93E-01	6.03E+02	2.79	-1.62E-01	4.80E+02	0.33	-4.66E-01	1.13E+01	0.46
S5	5	8.89E-01	4.18E+02	353.00	4.93E-01	-5.02E+01	74.75	3.77E-01	-6.53E+01	2.47	4.14E-01	1.26E+02	0.32	-8.14E-02	-4.04E+02	0.43
S6	6	1.39E+00	-3.67E+02	334.80	1.71E+00	-4.33E+02	71.58	7.68E-01	-4.62E+02	2.28	9.03E-01	-3.10E+02	0.30	4.08E-01	-6.39E+02	0.42
S7	7	5.04E-01	1.67E+01	343.70	8.79E-01	1.48E+02	76.39	3.07E-01	-6.71E+02	2.18	-1.18E-02	-5.55E+02	0.30	1.06E+00	-1.02E+03	0.40
S8	8	-1.37E+00	-1.43E+03	310.20	-3.12E-01	-1.30E+03	64.38	1.76E+00	-1.01E+03	2.02	1.76E+00	-8.82E+02	0.28	1.75E+00	-1.31E+03	0.38

Sample	Distance	Fe v(q)	Fe h(q)	Fe a(q)	Cu v(q)	Cu h(q)	Cu a(q)	Ni v(q)	Ni h(q)	Ni a(q)	Hg v(q)	Hg h(q)	Hg a(q)
S1	1	-5.85E-01	7.15E+02	23.28	-1.29E+00	3.55E+03	0.26	-1.27E+00	2.01E+03	0.19	-1.40E+00	-1.85E+02	0.63
S2	2	-8.13E-01	4.11E+02	22.27	-6.42E-01	-2.01E+02	0.24	-6.70E-01	-8.04E+01	0.17	-5.80E-01	-3.17E+02	0.60
S3	3	-8.14E-01	2.82E+02	21.84	1.18E-01	-3.95E+03	0.23	-1.15E-03	-1.53E+03	0.16	4.47E-01	2.04E+03	1.00
S4	4	-4.94E-01	-1.54E+01	20.85	4.78E-01	1.11E+04	0.28	2.98E-01	4.90E+03	0.20	6.44E-01	1.23E+03	0.86
S5	5	-1.94E-01	-1.75E+02	20.32	4.43E-01	5.96E+03	0.27	3.12E-01	2.65E+03	0.19	1.24E+00	-5.25E+01	0.65
S6	6	3.19E-01	-4.75E+02	19.32	-9.80E-01	6.70E+01	0.24	-8.03E-01	-8.04E+01	0.17	1.17E+00	-4.91E+02	0.57
S7	7	3.90E-01	-1.84E+01	20.84	1.36E-03	-4.76E+03	0.23	1.13E-01	-2.33E+03	0.16	-8.83E-01	-1.00E+03	0.49
S8	8	2.19E+00	-7.25E+02	18.49	1.87E+00	-1.17E+04	0.20	2.02E+00	-5.55E+03	0.14	-6.39E-01	-1.23E+03	0.45

Global: 72 | 30 | 41.7%

A: Param.	B: Cnt.	C: %
Hg	1	11.10%
Na, Cu, Ni, Hg	4	44.40%
Na, K, Pb, Cd, Cu, Ni, Hg	7	77.80%
Na, K, Pb, Cd, Cr, Fe, Hg	7	77.80%
Na, K, Pb, Cr, Fe	5	55.60%
Pb, Cd, Cr, Fe, Cu, Ni	6	66.70%

Source: Calculations made in TruVariogram software.

Regarding individual parameters, all ten contaminants identified by K. K. Pobi et al. as the most concerning (CN^-, Hg, Pb, Fe, Cr, Cd, Cu, Ni, COD, and Cl^-) are flagged as critical in at least three sampling points by the present methodology, confirming full agreement with the original authors' conclusions. Hg is critical from S3 to S6, consistent with Pobi et al.'s finding that mercury presents the highest contamination factor (CF) among heavy metals in the stream water. CN^- is critical at S5 through S7, and COD at S3 through S6, both aligned with the industrial discharge sources identified by the original investigators. Pb, Cd, and Cr are critical from S5 to S8, reflecting cumulative downstream accumulation from metal and chemical industry effluents. One parameter flagged by the present methodology that was not highlighted by Pobi et al. is NO_3^-, identified as critical at S2, S3, and S6. This discrepancy is expected, due to Pobi et al. focused on industrial heavy metal sources, whereas nitrate variability may reflect mixed contributions from domestic wastewater associated with the Gopalpur population settlement located along the riverbank, which the variographic approach captures independently of source attribution.

The positive heterogeneity observed for BOD and COD at S6 and S7 —indicating that local concentrations exceed the weighted batch mean— provides additional evidence of active organic loading at those points, consistent with the proximity of chemical and pharmaceutical facilities. Taken together, the VCC-based evaluation not only reproduces the critical parameters and points identified by Pobi et al. through pollution indices and enrichment factors but also quantifies the spatial gradient of contamination from the upstream baseline to the most industrially impacted zone, providing a basis for prioritizing future field investigations.

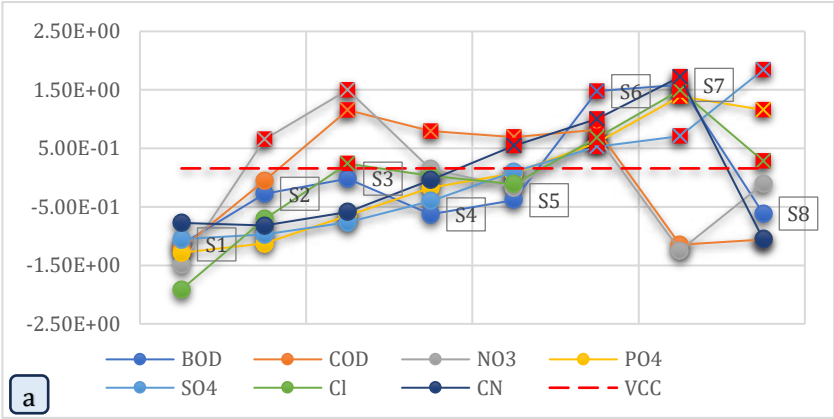

(a) Composite variogram for the group of anions, BOD, and COD.

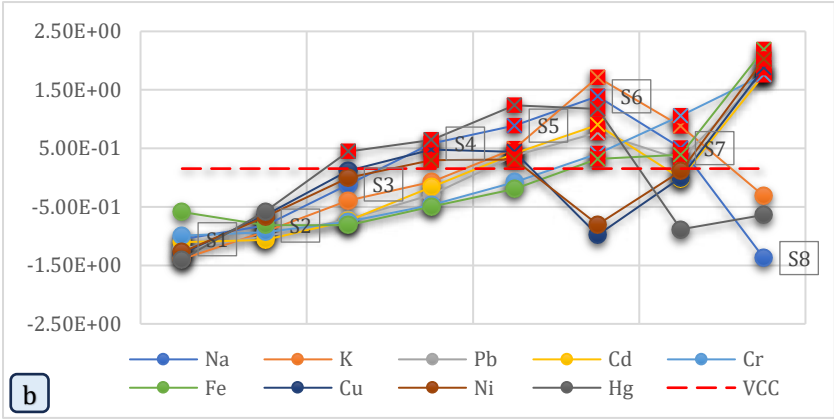

(b) Composite variogram for the group of cations.

In both variograms, the x-axis labels from S1 to S8 indicate the sampling point associated with each variance value via the relationship $v(q) = v(j-1)$ (Equation 14). Red squares marked with an "X" indicate normalized variance values $v(j)_{Norm}$ exceeding the defined VCC_{Norm}.

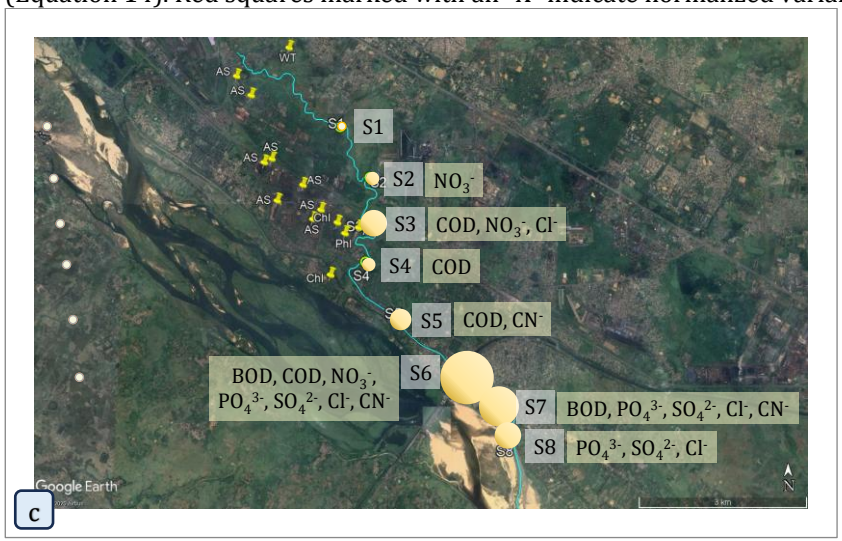

(c) Critical points evaluation map for anions, BOD, and COD.

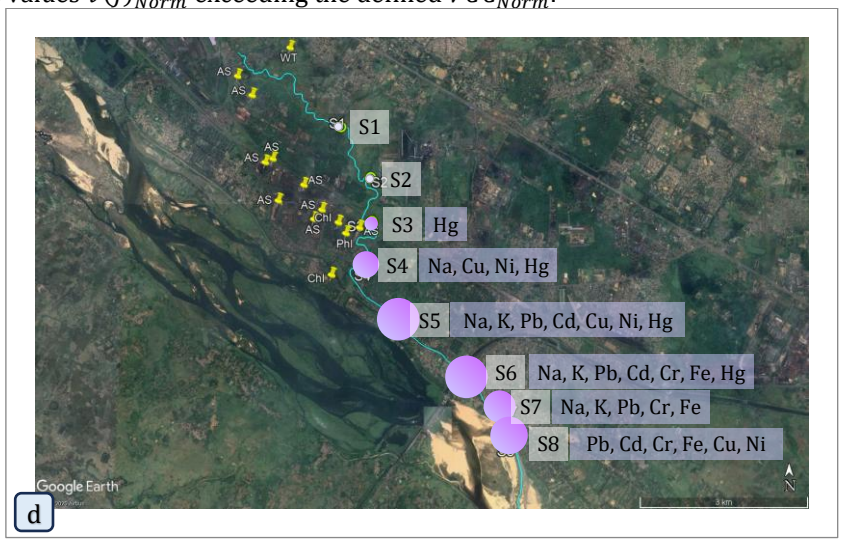

(d) Critical points evaluation map for cations.

Note: Reference points for industrial and commercial activities identified using Google Earth were added. Abbreviations: AS: steel and/or metal industry; WT: water treatment plant; ChI: chemical industry; PhI: pharmaceutical industry.

Figure 2. Composite normalized variograms and maps highlighting critical points obtained from the study by K. K. Pobi et al. (Pobi et al., 2019) on the Tamla Nala stream, Durgapur industrial zone, India. A normalized VCC_{Norm} of 0.158 (anion/BOD/COD group) and 0.154 (cation group) were applied.

Source: Author's own elaboration based on TruVariogram software. Satellite images from Google Earth, 2025.

2. Joanna Jaskuła et.al. in 2021: "Analysis of Spatial Variability of River Bottom Sediment Pollution with Heavy Metals and Assessment of Potential Ecological Hazard for the Warta River, Poland".

The article by (Jaskuła et al., 2021) evaluates the contamination of bottom sediments in the Warta River, Poland, with heavy metals (Cr, Ni, Cu, Zn, Cd, and Pb). The river faces a significant environmental issue due to intensive anthropogenic pressure: its catchment area covers approximately 17.4% of Poland's territory, with agriculture as the dominant land use and urban centers along its course acting as point sources of contamination. A total of 24 sample collection stations were monitored along the full length of the river in 2016 and 2017. Analysis using the Geoaccumulation Index (Igeo), Enrichment Factor (EF), Pollution Load Index (PLI), and Metal Pollution Index (MPI) demonstrated heavier contamination in 2016 than in 2017. Assessment of potential toxic effects based on the Threshold Effect Concentration (TEC), Midpoint Effect Concentration (MEC), Probable Effect Concentration (PEC), and the Toxic Risk Index (TRI) indicated a substantially lower ecological hazard in 2017. Cluster analysis identified two main groups of stations with similar chemical profiles, suggesting that point sources in urbanized areas and river fluvial processes are the primary drivers of heavy metal distribution.

For evaluation using the proposed methodology, only the VCC_{Norm} criterion was applied. A VCC_{Norm} of 0.215 was used for the 2016 dataset and 0.204 for 2017, both derived from the empirical estimator (Equation 7) applied to the respective composite variograms. No heterogeneity criteria were applied, nor was an explicit identification of concentrations before and after detected critical points conducted. The results are presented in Table s.2, Table s.3 and Figure s.1 in Supplementary Information.

Of the 144 parameter-point combinations evaluated for 2016 (6 parameters × 24 stations), 39 were identified as critical, corresponding to 27.1%. For 2017, 43 combinations were critical, corresponding to 29.9% —a slight increase that reflects a shift in the spatial distribution of contamination rather than an overall improvement. The full breakdown by station is presented in Table s.1.

The spatial pattern in 2016 is concentrated in the lower course of the river. Stations p1 through p17 are largely non-critical, with isolated flags at p1 (Ni, Pb, Zn), p8 (Zn), p13 (Zn), and p15–p17 (Cu, Pb, Zn in varying combinations). From p18 onward, the number of critical parameters rises sharply: p18 flags Cd, Cr, Cu, Pb, and Zn; p19 flags Cd, Cu, Ni, Pb, and Zn; p21 is the most heavily impacted station, with all six parameters critical (100%). This spatial clustering in the lower course is consistent with the findings of Jaskuła et al., who identified stations below the city of Poznań —the largest city on the river— as forming a distinct high-contamination group in the cluster analysis, and who attributed elevated PLI and MPI values in that section to point sources from urbanized areas.

The 2017 pattern is markedly different. Station p1, which was critical for Ni, Pb, and Zn in 2016, shows no critical parameters in 2017, consistent with the reduction in Cr and Pb concentrations at that station documented by Jaskuła et al. In contrast, Cd emerges as a dominant critical parameter across the middle course: it is flagged at 11 of the 24 stations (p5, p10 through p19), a distribution not observed in 2016. This is consistent with the finding by Jaskuła et al. that the differences in Cd concentrations between the two years were statistically insignificant by the Kruskal–Wallis test, while its spatial spread increased —suggesting that Cd sources became more distributed along the river rather than concentrated at specific points. Cu is the most widespread critical parameter in 2017, flagged at 12 of the 24 stations. The lower course remains critical (p21-p24), now dominated by Cr, Cu, Ni, Pb, and Zn rather than Cd as in 2016, reflecting the shift in the contamination profile documented by the original authors.

The slight increase in the global percentage of critical parameter-point combinations from 27.1% in 2016 to 29.9% in 2017 —despite an overall reduction in mean concentrations— is explained by the expanded spatial reach of Cd and Cu in 2017. This finding is consistent with the observation by Jaskuła et al. that the differences between years were statistically significant for Cr, Ni, and Pb but not for Cd and Cu, indicating that the latter two metals maintained persistent or broadened spatial influence. The variographic methodology thus captures a nuance that global indices tend to obscure, i.e. overall contamination can decrease while the number of spatially affected stations increases, if the distribution of remaining contamination becomes more diffuse.

The conclusions drawn from the VCC_{Norm}-based evaluation are in agreement with those of Jaskuła et al., i.e. contamination is most severe in the lower course of the Warta River, point sources in urbanized areas are the primary drivers, and the lower overall contamination in 2017 coexists with persistent Cd and Cu pressure across a broader section of the river. An additional insight provided by the present methodology is the spatial resolution at the individual station level —identifying p21 as the single most impacted station in 2016 and quantifying the upstream spread of Cd in 2017— which complements the group-level characterization offered by cluster analysis. Based on the above, future monitoring campaigns for the Warta River should maintain sampling density in the lower course (from p18 onward) and expand Cd monitoring to the middle course stations p10-p17, where the variographic analysis suggests an emerging and diffuse contamination pattern.

3. Werner Brack et.al. in 2007: "Polychlorinated naphthalenes and other dioxin-like compounds in the Elbe River sediments.".

Following the 500-year flood of the Elbe River in 2002, contamination of river sediments by dioxin-like compounds was investigated by (Brack et al., 2008), with particular focus on polychlorinated naphthalenes (PCNs), which had not previously been analyzed in this river system. The study combined the H4IIE-luc bioassay for total aryl hydrocarbon receptor (AhR)-mediated activity with congener-specific chemical analyses of polychlorinated biphenyls (PCBs), polychlorinated dibenzo-p-dioxins and dibenzofurans (PCDD/F), and PCNs at nine stations along the German stretch of the Elbe River. Toxicity was expressed as Toxic Equivalent Quantities (TEQ) normalized to both dry weight (dw) and total organic carbon (toc). For the variographic evaluation, only the TOC-normalized expressions are used, as they account for differences in organic matter content between sampling sites and provide the most environmentally relevant basis for spatial comparison.

Brack et al. concluded that PCDD/F dominated dioxin-like activity in the central and lower Elbe River, with Bitterfeld as the primary contamination source. PCNs were detected throughout the German stretch — representing the first documented occurrence in this system— with concentrations increasing from less than 1 ng TEQ/kg TOC upstream of Bitterfeld to more than 240 ng TEQ/kg TOC at Magdeburg (MAG) and declining sharply at Arneburg (ARN) and Hitzacker (HIT). PCBs contributions were diffuse and of lesser magnitude. Königstein (KON) and Dresden (DRE), located upstream near the Czech border, showed the lowest overall contamination.

For evaluation using the proposed methodology, only the VCC_{Norm} criterion was applied. A VCC_{Norm} of 0.173 was derived from the empirical estimator (Equation 7) applied to the composite TOC-normalized variogram. No heterogeneity criteria were applied, nor was an explicit identification of concentrations before and after detected critical points conducted. Of the 27 parameter-site combinations evaluated (3 parameters × 9 stations, TOC basis), 14 were identified as critical, corresponding to 51.9%. The results are presented in Table s.4 and Figure s.2 in Supplementary Information.

The spatial pattern produced by the VCC_{Norm} evaluation is in full agreement with the conclusions of Brack et al. KON and DRE are non-critical for all three compound classes, consistent with their characterization as relatively uncontaminated upstream reference sites. From Torgau (TOR) onward —immediately downstream of the Bitterfeld industrial zone— all three parameters (PCB_{toc}, $PCDD/F_{toc}$, $PCNs_{toc}$) are flagged as critical, reflecting the documented mobilization and downstream transport of contaminated sediments following the 2002 flood. This three-parameter criticality is maintained at LEO and BAR, which are the stations closest to the Bitterfeld contamination plume in central Elbe. At MAG, PCDD/F and PCNs remain critical while PCBs drop below the threshold, consistent with the finding by Brack et al. that PCBs activity was more diffuse and less linked to the Bitterfeld point source. ARN is non-critical for all parameters, confirming the recovery of the river from PCDD/F and PCNs contamination observed at that station. HIT flags only PCBs as critical, consistent with the anomalously high PCB-mediated TCDD-equivalent concentrations at that site reported by Brack et al. —the highest recorded in the entire study— attributed to diffuse inputs rather than Bitterfeld.

The VCC_{Norm}-based evaluation thus reproduces, at the individual station level, the full spatial narrative described by Brack et al.: contamination originates in the Bitterfeld region, propagates downstream through TOR, WIT, LEO, BAR, and MAG, reaches a recovery point at ARN, and reappears at HIT through a distinct PCB-dominated mechanism. This spatial correspondence, achieved without recourse to TEQ thresholds, regulatory standards, or source attribution models, demonstrates the capacity of the variographic methodology to characterize complex contamination gradients in river systems affected by episodic events such as major floods.

For future monitoring, the results reinforce the recommendation of Brack et al. to include PCNs alongside PCDD/F and PCBs in routine Elbe River assessments. The variographic analysis additionally suggests that sampling efforts should focus on the TOR–MAG corridor as a high-priority zone, while KON and DRE could serve as upstream reference stations given their consistently non-critical status. ARN merits continued monitoring as the documented recovery boundary for PCDD/F and PCNs contamination.

4. Study of Sediments in the Orckojahuira River Segment Between the Incachaca Dam and the Initial Sector of La Paz City, Bolivia.

General description

The Orckojahuira River is located in the La Paz Department of Bolivia and constitutes a sub-basin of the Choqueyapu River system, the primary waterway of La Paz city. The studied segment extends from the Incachaca Dam —a key water supply infrastructure with a storage capacity of 4.2 million m^3 (AAPS - PERIAGUA III, 2022)— to the Chuquiaguillo area at the city's initial urban fringe, covering approximately 27.9 km of river

length. This segment was selected because mineral ore processing plants located along its banks discharge tailings directly into the riverbed, enabling both visual identification of contamination sources and direct comparison between field-based and variography-based critical point identification.

Geological and hydrological setting

The Orckojahuira region lies within the Andean Altiplano, a high plateau characterized by complex geology comprising volcanic and sedimentary rocks —basalts, andesites, and lacustrine sediments— overlain by glacial deposits associated with at least 15 documented glacial events during the late Pliocene and early Pleistocene (Roberts, 2016). The river originates in the Cordillera Real under the name Chuquiaguillo and flows through steep, incised valleys shaped by combined fluvial and glacial erosion. Its proximity to Mount Chacaltaya — whose 18,000-year-old glacier fully melted by 2009— suggests that the area's sediments include historical glacial material that may contribute background concentrations of lithogenic elements.

The river's hydrology is governed by its high-altitude origin and a pronounced seasonal regime with distinct wet and dry seasons. Flow is sustained primarily by precipitation and snowmelt (Liberman et al., 2021), with evapotranspiration rates in the upper basin reaching values typical of high-altitude Andean systems (Ibañez Apaza, 2022). In addition to natural inputs, the river receives urban sewage and mining-derived wastewater, rendering it a compound receptor of both diffuse and point-source contamination. The only prior chemical characterization of river water quality was conducted in 2010, involving six samples collected within the La Paz Municipality (Huallpara Lliully et al., 2010); the present study constitutes the first variography-based sediment assessment for this system.

Description of the river segment and sampling points

Sediment samples were collected in September 2021 and September 2024, a few weeks before Bolivia's rainy season, to minimize the influence of flood-driven sediment transport on the spatial distribution of contaminants. At each of the eight designated stations, two samples were collected to assess vertical contaminant distribution: a surface sample (0–5 cm depth), reflecting recent contaminant inputs, and a deep sample (5–15 cm), providing insights into historical deposition patterns.

Stations were distributed strategically along a gradient from upstream reference conditions to areas directly influenced by ore processing activities (Figure 3, Figure 4 and Table 4). O1, located immediately downstream of the Incachaca Dam, serves as the head of the segment and exhibits minimal anthropogenic influence; its sediments are of clayey character and emit a sulfurous odor indicative of anaerobic decomposition under anoxic conditions. O2 is similarly unaffected by mining operations and provides a secondary baseline. From O3 onward, stations are positioned alternately downstream of each ore processing plant (OPP1 through OPP4) and in intermediate zones between facilities, following the sequence: O3 (downstream of OPP1 via a tributary), O4 (downstream of OPP2), O5 (downstream of OPP3), O6 (upstream of OPP4, but exposed to cumulative upstream discharges), O7 (downstream of OPP4), and O8 (within the Chuquiaguillo urban area, capturing the integrated downstream signal). A summary of each station's location, sediment characteristics, and preliminary field-based classification as critical or non-critical is provided in Table 4.

The spatial arrangement of stations, alternating between direct discharge zones and intermediate reaches, is designed to allow the variographic methodology to detect both the immediate impact of each point source and the cumulative downstream accumulation of contaminants. A pattern that the field observations, summarized in Table 4, predicted to be concentrated from O3 through O8.

XRF analysis and quality control

Collected sediment samples were air-dried at room temperature and manually disaggregated prior to analysis in triplicate by X-ray fluorescence (XRF) using a portable Thermo Scientific Niton XL3t-950 analyzer equipped with a Soils module and main, high, and low energy filters, with an acquisition time of 30 seconds per filter.

To ensure result reliability, the instrument's factory-preset calibration curves were adjusted using certified reference materials (CRMs) and regression models of the form $\mathbf{Y} = \mathbf{X} \cdot \boldsymbol{\beta} + \boldsymbol{\epsilon}$, fitted as linear, quadratic, or cubic functions depending on the analyte and concentration range. Confidence and prediction bands were calculated for each calibration curve following the methodology described in (Romero Prieto & Guzmán Alegria, 2024), providing a quantitative measure of the uncertainty associated with the analytical technique, the sample matrix, and the preparation procedure. These bands were used to assess each regression model's ability to predict concentrations in unknown samples of comparable matrix composition, and to confirm that the reported concentrations fall within the reliable working range of the instrument for each element.

Figure 3. Upstream perspective view (toward the Incachaca Dam) of sampling points and reference locations.
Source: Authors' own elaboration. Satellite images from Google Earth, 2025.

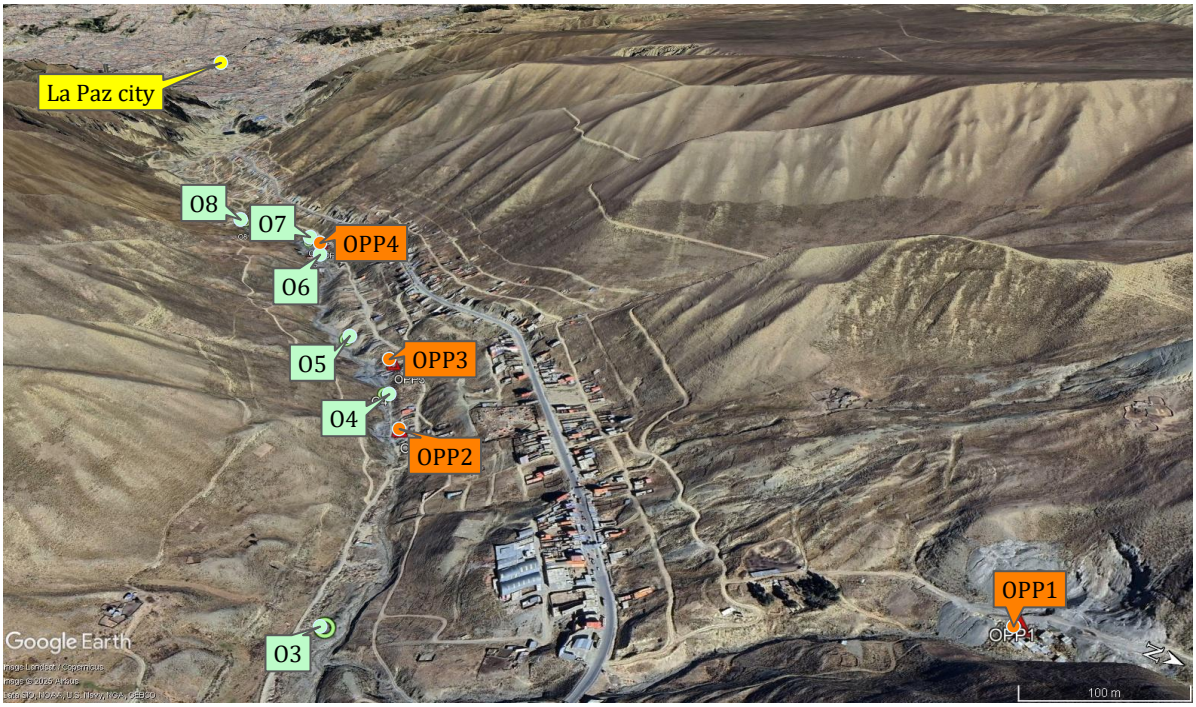

Figure 4. Downstream perspective view (toward La Paz city) of sampling points and reference locations.
Source: Authors' own elaboration Satellite images from Google Earth, 2025.

Table 4. Sampling points and mineral processing plants in the study segment of the Orckojahuira River (between the Incachaca Dam and the initial sector of La Paz city).

Sample point	Description	Evaluation
O1	Head of the basin segment. Upstream lies the Incachaca Dam, which stores water for purification and distribution to La Paz city. Surrounding areas include livestock and some grasslands. Sediment samples exhibit clayey characteristics. Additionally, the sediment is waterlogged and emits a strong odor of decomposing organic matter.	Head of the segment with little to no anthropogenic influence.
O2	Near a dirt road. A structure belonging to EPSAS (Public Social Water and Sanitation Company of La Paz) is present. Collected sediments consist of a clay-sand mixture.	Point with minimal anthropogenic influence.
O3	Approximately 10 m from a tributary to the Orckojahuira River receiving direct discharges from a mineral processing plant (OPP1). Collected materials contain little clay and are predominantly sandy.	Critical point. Influenced by discharges from OPP1 via a tributary.
O4	Approximately 150 m downstream of OPP2. Sample colors range from brown to gray tones, with a predominantly sandy texture.	Critical point. Influenced by discharges from OPP2.
O5	Approximately 150 m downstream of OPP3. Samples exhibit a grayish color and a predominantly sandy texture.	Critical point. Influenced by discharges from OPP3.
O6	Approximately 150 m upstream of OPP4. Samples are dark gray with a sandy texture.	Critical point. Influenced by discharges from OPP3.
O7	Approximately 150 m downstream of OPP4. Samples are dark gray with a sandy texture.	Critical point. Influenced by discharges from OPP4.
O8	Approximately 350 m downstream of O7. This point is influenced by discharges from upstream mineral processing plants. Samples are dark gray with a sandy texture.	Critical point. Influenced by upstream discharge activities.

Source: Authors' own observations during sample collection activities.

Application of the VCC_{Norm} methodology and evaluation

The evaluation of sediment samples from the Orckojahuira River was conducted using the VCC_{Norm} criterion exclusively. The VCC_{Norm} values were derived from the empirical estimator (Equation 7) applied to each composite normalized variogram: 0.154 for surface sediments in the 2021 campaign, 0.156 for surface sediments in 2024, 0.155 for deep sediments in 2021, and 0.156 for deep sediments in 2024. No heterogeneity criteria were applied, nor was an explicit identification of concentrations before and after the detected critical points performed.

Results for surface sediments are presented in Table 5 and Table 6, corresponding to the 2021 and 2024 campaigns respectively. Results for deep sediments are presented in Table 7 and Table 8. The spatial distribution of critical parameters is illustrated through composite normalized variograms and georeferenced maps in Figure 5 and Figure 6.

Surface sediments

Of the 112 parameter-point combinations evaluated for surface sediments in 2021 (14 parameters × 8 stations), 39 were identified as critical, corresponding to 34.8%. In 2024, 41 combinations were critical (36.6%), indicating a modest but consistent increase in contamination pressure over the three-year period between campaigns. The spatial pattern in both surface campaigns exhibits a clear downstream intensification. Stations O1 and O2 —located upstream of mining influence and in an area of minimal anthropogenic disturbance respectively— show zero or one critical parameter, consistent with their characterization as baseline reference points (Table 4). From O3 onward, the number of critical parameters increases progressively with proximity to ore processing plants. In 2021, O7 is the most severely impacted station with 12 critical parameters (85.7%),

encompassing S, Ca, Ti, V, Cr, Mn, Fe, Ni, Cu, As, Ba, and Pb; O8 follows with 11 (78.6%). In 2024, both O6 and O7 reach 12 critical parameters (85.7%), reflecting an upstream shift in the peak contamination zone consistent with the documented increase in mining activity.

Sulfur and calcium are the most spatially consistent critical parameters across both surface campaigns, flagged at O5 through O7 in 2021 and at O6 through O8 in 2024. The prominence of sulfur reflects the input of pyrite-bearing tailings (FeS_2) from mineral processing plants, corroborated by the sulfurous odor recorded organoleptically at O1 and the progressive increase from O4 onward. Calcium variations are attributed to the use of slaked lime ($Ca(OH)_2$) as an alkalizing agent in flotation circuits —a standard practice for lead and silver ore processing— which introduces elevated calcium to the river along with the ore-processing discharges.

Arsenic, lead, and barium are consistently critical at O6–O8 in both campaigns, underscoring the accumulation of tailings-associated metals in the lower segment of the studied reach. The appearance of additional elements —including nickel, manganese, and iron— at O7 and O8 in both campaigns reflects the cumulative effect of multiple upstream processing plants on sediment composition. Lead concentrations at O7 and O8 in 2024 exceeded 3800 $mg \cdot kg^{-1}$ and 1300 $mg \cdot kg^{-1}$ respectively, compared to approximately 30 $mg \cdot kg^{-1}$ at O1, a 127-fold increase that underscores the severity of downstream contamination and the absence of effective mitigation between campaigns.

Deep sediments

Of the 112 parameter-point combinations evaluated for deep sediments in 2021, 42 were critical (37.5%). The same percentage was obtained in 2024 (42/112, 37.5%), though the identity of critical parameters shifted substantially between campaigns, reflecting changes in the composition and intensity of tailings discharges over the three-year period.

In the 2021 deep campaign, the upstream stations O2 and O3 already flag potassium, copper, and barium as critical —an early signal not observed in the surface sediments of the same campaign— suggesting that these elements had already begun accumulating at depth before the full spatial gradient of surface contamination developed. Chromium is critical at four stations in 2021 (O1, O4, O6, O7), with an anomalous flag at O1 that may reflect background geological contributions from chromium-bearing volcanic and sedimentary rocks characteristic of the Andean substrate. From O5 onward, sulfur, calcium, lead, arsenic, and zinc are consistently critical, confirming the dominant influence of tailings from OPP3 and OPP4 at depth.

In the 2024 deep campaign, the spatial pattern is notably cleaner: O1 through O3 show no critical parameters, and O4 flags only chromium. From O5 onward the contamination intensifies markedly, with O7 reaching 13 critical parameters (92.9%) —the highest value across all four datasets— and O8 flagging 12 (85.7%). This pattern, combined with the 2021 observation of early-appearing potassium and copper at O2–O3, is consistent with a model of progressive sediment column saturation: by 2024, shallow-depth signals have become surface-level, while the deep layer at the upper stations has been partially flushed or diluted by cleaner upstream inputs during the three-year interval.

Lead in deep sediments is particularly striking in 2024, with concentrations at O7 and O8 exceeding 2200 $mg \cdot kg^{-1}$ and 3200 $mg \cdot kg^{-1}$ respectively, compared to approximately 80 $mg \cdot kg^{-1}$ and 120 $mg \cdot kg^{-1}$ at the same stations in 2021. This three-year increase of more than 25-fold at O8 is consistent with intensified processing of galena-rich (PbS) ores, which generate lead-bearing tailings as a primary byproduct.

Validation against field observations and predictive utility

The VCC_{Norm}-based evaluation is in full agreement with the preliminary field classifications presented in Table 4. Stations O3 through O8, characterized as critical based on proximity to ore processing plants and direct visual evidence of tailings discharge, are identified as critical by the variographic methodology in all four datasets. Stations O1 and O2, classified as non-critical or baseline references in the field assessment, show zero or minimal critical parameters across all campaigns —with the exception of the anomalous Cr flag at O1 (deep, 2021) discussed above.

As a predictive tool, the 2021 variographic analysis correctly anticipated that the contamination gradient from O4 to O8 warranted intensified monitoring in subsequent campaigns. The 2024 results confirmed this prediction: the number of critical parameters increased at all stations from O5 onward, and lead emerged as a widespread critical element throughout the deep sediment column. The methodology additionally identifies O8 —the most downstream station in the studied segment— as the point where maximum accumulation of multiple contaminants occurs, recommending the establishment of at least two additional sampling stations downstream to characterize the full spatial extent of contamination before its confluence with the urban Choqueyapu River system.

Table 5. Calculated normalized variance values $v(j)_{Norm}$ and critical point evaluation based on parameters $a(q)$ analyzed for the Orckojahuira River, Bolivia. **Surface sediment** samples from the 2021 campaign (1st campaign). A VCC_{Norm} of 0.154 was applied. The evaluation comprises 112 parameter-point combinations (14 parameters × 8 sampling stations).

	Minigraph																		
	v(j)/h(q)/a(q)	*v(j)*	*h(q)*	*a(q)*	*v(j)*	*h(q)*	*a(q)*	*v(j)*	*h(q)*	*a(q)*	*v(j)*	*h(q)*	*a(q)*	*v(j)*	*h(q)*	*a(q)*	*v(j)*	*h(q)*	*a(q)*
Sample	**Distance**	**S**			**K**			**Ca**			**Ti**			**V**			**Cr**		
O1s	1	-3.21E-01	-1.74E+03	14234.89	-1.26E+00	-1.37E+02	28448.25	-8.46E-01	-3.78E+01	9680.25	-8.52E-01	6.40E+02	6138.11	5.88E-01	2.86E+02	187.89	-1.27E+00	9.44E+02	100.61
O2s	2	-7.32E-01	1.31E+03	1986.55	-2.00E-01	9.45E+01	28722.02	-1.06E+00	6.60E+02	1973.06	-8.76E-01	9.81E+02	6455.39	-6.20E-01	2.48E+02	185.08	-9.22E-01	6.28E+02	94.14
O3s	3	-6.94E-01	1.46E+03	1379.10	1.30E+00	-9.48E+02	27491.83	-1.01E+00	6.66E+02	1897.15	-6.88E-01	5.17E+02	6024.50	-1.12E+00	1.98E+02	181.41	-5.93E-01	9.08E+02	99.87
O4s	4	-6.62E-03	1.30E+03	2016.81	1.47E+00	-1.52E+03	26821.53	-4.57E-01	6.51E+02	2069.90	-4.81E-01	-3.08E+02	5256.15	-5.79E-01	-2.81E+01	164.73	-3.56E-01	2.27E+02	85.91
O5s	5	5.14E-01	7.08E+02	4403.27	1.83E-01	2.80E+02	28941.28	1.71E-01	2.09E+02	6950.42	-4.22E-01	-1.88E+01	5525.62	-6.12E-01	7.95E+01	172.66	3.31E-01	-8.98E+02	62.85
O6s	6	6.06E-01	-4.32E+02	8977.69	-2.95E-01	1.53E+03	30411.38	4.98E-01	-2.97E+02	12545.99	3.59E-01	-2.12E+02	5345.91	3.39E-02	-3.20E+02	143.20	6.28E-01	-6.70E+02	67.52
O7s	7	1.91E+00	3.75E+02	5740.51	-2.41E-02	1.61E+03	30509.51	1.30E+00	-3.38E+01	9636.81	1.24E+00	-3.34E+02	5232.13	2.51E-01	2.40E+02	184.50	3.29E-01	-1.50E+02	78.19
O8s	8	-1.27E+00	-2.99E+03	19229.30	-1.18E+00	-9.09E+02	27537.66	1.40E+00	-1.82E+03	29349.61	1.72E+00	-1.26E+03	4366.83	2.06E+00	-7.04E+02	114.96	1.86E+00	-9.89E+02	60.98

	Minigraph																		
	v(j)/h(q)/a(q)	*v(j)*	*h(q)*	*a(q)*	*v(j)*	*h(q)*	*a(q)*	*v(j)*	*h(q)*	*a(q)*	*v(j)*	*h(q)*	*a(q)*	*v(j)*	*h(q)*	*a(q)*	*v(j)*	*h(q)*	*a(q)*
Sample	**Distance**	**Mn**			**Fe**			**Ni**			**Cu**			**Zn**			**As**		
O1s	1	-6.37E-01	8.44E+02	179.29	-7.64E-01	1.61E+03	59512.55	-9.36E-01	2.62E+03	0.00	-1.21E+00	1.98E+03	40.06	2.13E+00	-8.81E+00	291.77	-2.03E-01	2.53E+02	64.40
O2s	2	-5.40E-01	4.59E+02	373.54	-7.13E-01	-2.20E+02	28182.52	-7.38E-01	9.36E+02	32.78	-4.76E-01	3.59E+03	38.10	-2.29E-01	-4.26E+02	399.57	-9.00E-01	3.15E+02	44.02
O3s	3	-5.53E-01	-2.88E+02	750.74	-5.93E-01	-2.52E+02	27641.41	-5.59E-01	-3.97E+02	58.78	2.56E-01	-4.50E+03	47.91	-9.48E-01	-8.66E+01	311.87	-1.13E+00	3.22E+02	41.41
O4s	4	-5.41E-01	1.40E+02	534.64	-3.85E-01	-3.38E+02	26171.61	-5.83E-01	8.29E+02	34.88	1.22E-02	-1.08E+02	42.59	3.27E-01	-5.11E+02	421.50	-5.35E-01	3.30E+02	38.91
O5s	5	-2.58E-01	1.52E+02	528.56	-1.40E-01	-3.81E+02	25429.84	-1.39E-01	-3.33E+02	57.53	-5.29E-01	3.19E+03	38.59	-1.49E-01	3.65E+02	195.26	-8.41E-02	1.73E+02	90.95
O6s	6	-1.86E-01	-4.25E+02	820.02	-1.86E-01	-8.64E+01	30465.55	1.11E-01	-9.82E+02	70.18	-7.88E-01	5.90E+03	35.30	2.85E-02	-3.25E+01	297.90	2.84E-01	-4.71E+02	304.90
O7s	7	3.79E-01	9.61E+01	556.79	5.27E-01	-1.77E+02	28914.01	7.70E-01	-1.08E+03	72.16	8.31E-01	1.39E+02	42.29	5.02E-03	5.35E+02	151.30	5.13E-01	5.49E+01	130.29
O8s	8	2.34E+00	-9.78E+02	1098.77	2.25E+00	-1.60E+02	29210.46	2.07E+00	-1.59E+03	81.98	1.91E+00	-1.02E+04	54.82	-1.17E+00	1.65E+02	246.74	2.06E+00	-9.78E+02	473.31

	Minigraph									
	v(j)/h(q)/a(q)	*v(j)*	*h(q)*	*a(q)*	*v(j)*	*h(q)*	*a(q)*		Global: 112	39
Sample	**Distance**	**Ba**			**Pb**			**A: Param.**		*34.8%*
									B: Cnt.	**C: %**
O1s	1	-5.42E-01	1.23E+03	6087.66	-8.77E-01	4.77E+02	47.96	V, Zn	2	14.30%
O2s	2	-6.54E-01	-1.36E+02	2284.81	-1.24E+00	3.40E+02	56.16			
O3s	3	-6.01E-01	-1.13E+02	2350.11	-9.18E-01	4.67E+02	48.52	K, Cu	2	14.30%
O4s	4	-4.09E-01	-2.47E+02	1977.81	-1.52E-01	3.46E+02	55.80	K, Zn	2	14.30%
O5s	5	-3.35E-01	-1.74E+02	2179.56	2.13E-02	4.95E+02	46.89	S, K, Ca, Cr	4	28.60%
O6s	6	-1.44E-01	-1.25E+02	2314.11	7.49E-01	-6.26E+02	114.23	S, Ca, Ti, Cr, As, Pb	6	42.90%
O7s	7	3.40E-01	-1.44E+02	2261.79	8.01E-01	-6.35E+02	114.72	S, Ca, Ti, V, Cr, Mn, Fe, Ni, Cu, As, Ba, Pb	12	85.70%
O8s	8	2.35E+00	-2.96E+02	1841.78	1.62E+00	-8.64E+02	128.50	Ca, Ti, V, Cr, Mn, Fe, Ni, Cu, As, Ba, Pb	11	78.60%

Source: Calculations made in TruVariogram software.

Table 6. As Table 5, for surface sediment samples from the 2024 campaign (2nd campaign). A VCC_{Norm} of 0.156 was applied.

	Minigraph																		
	v(j)|h(q)|a(q)	*v(j)*	*h(q)*	*a(q)*	*v(j)*	*h(q)*	*a(q)*	*v(j)*	*h(q)*	*a(q)*	*v(j)*	*h(q)*	*a(q)*	*v(j)*	*h(q)*	*a(q)*	*v(j)*	*h(q)*	*a(q)*
Sample	**Distance**	**S**			**K**			**Ca**			**Ti**			**V**			**Cr**		
O1s	1	-1.29E+00	2.16E+03	1613.76	-1.27E+00	4.01E+03	23990.76	-8.86E-01	-7.68E+02	2727.26	-1.34E+00	-1.29E+03	6174.20	-8.67E-01	-4.61E+02	145.46	-2.24E-02	-4.91E+02	86.70
O2s	2	-9.56E-01	2.47E+03	0.00	-1.92E-01	-1.36E+04	32580.36	-1.24E+00	-7.69E+02	2695.90	-9.44E-01	-3.20E+03	7939.25	-1.01E+00	-9.85E+02	180.10	-1.30E+00	-9.00E+02	101.36
O3s	3	-6.31E-01	2.36E+03	594.02	1.83E-01	-9.15E+03	30396.42	1.58E-04	-7.46E+02	3257.38	-4.15E-01	-1.20E+03	6090.70	-7.79E-01	-6.36E+02	157.03	-4.22E-01	-4.24E+02	84.30
O4s	4	-4.07E-01	1.97E+03	2632.68	-4.76E-01	5.89E+03	23076.79	1.62E+00	8.58E+02	43008.22	-2.18E-01	1.67E+03	3456.10	-4.50E-01	5.98E+02	75.45	1.66E+00	7.21E+02	43.28
O5s	5	6.65E-02	8.39E+02	8534.21	7.46E-02	-1.23E+03	26540.81	1.09E+00	6.73E+02	38427.29	-1.10E-01	5.76E+02	4460.07	-3.63E-01	-1.74E+02	126.47	1.01E+00	3.39E+02	56.97
O6s	6	6.23E-01	1.55E+03	4818.46	1.35E+00	7.52E+02	25577.27	5.13E-01	6.46E+02	37753.75	8.29E-01	7.44E+02	4305.42	9.79E-01	3.97E+02	88.78	4.27E-01	7.62E+02	41.81
O7s	7	1.53E+00	-6.16E+03	45179.83	1.43E+00	5.56E+03	23236.48	-5.90E-01	3.75E+01	22685.16	1.79E+00	1.10E+03	3976.83	1.60E+00	4.66E+02	84.17	-3.14E-01	-2.28E+02	77.28
O8s	8	1.06E+00	-5.18E+03	40052.61	-1.10E+00	7.80E+03	22147.33	-5.09E-01	6.98E+01	23485.12	4.08E-01	1.60E+03	3520.90	8.89E-01	7.94E+02	62.50	-1.04E+00	2.21E+02	61.19

	Minigraph																		
	v(j)|h(q)|a(q)	*v(j)*	*h(q)*	*a(q)*	*v(j)*	*h(q)*	*a(q)*	*v(j)*	*h(q)*	*a(q)*	*v(j)*	*h(q)*	*a(q)*	*v(j)*	*h(q)*	*a(q)*	*v(j)*	*h(q)*	*a(q)*
Sample	**Distance**	**Mn**			**Fe**			**Ni**			**Cu**			**Zn**			**As**		
O1s	1	-1.34E+00	9.73E+02	1423.36	-1.49E+00	2.18E+03	52369.79	-1.11E+00	2.69E+03	45.06	1.20E+00	5.52E+02	36.52	-2.44E-02	4.04E+02	252.79	-1.39E+00	3.64E+03	68.36
O2s	2	-5.52E-01	-9.13E+03	955.47	-8.89E-01	-2.07E+02	65303.29	-9.12E-01	3.69E+03	37.68	-1.96E-01	-1.28E+02	61.30	-7.50E-01	4.12E+02	245.10	-9.74E-01	3.56E+03	107.75
O3s	3	2.32E-02	-1.47E+04	698.71	-2.08E-01	5.96E+02	60957.20	-7.64E-01	3.15E+03	41.62	-7.47E-01	3.52E+01	55.37	-9.15E-01	3.20E+02	333.65	-5.31E-01	3.63E+03	73.57
O4s	4	-3.67E-01	1.82E+03	1462.40	1.32E-01	4.26E+03	41126.72	-5.29E-01	-8.75E+00	64.81	-7.14E-02	7.20E+02	30.43	-3.02E-01	5.50E+02	112.27	-2.97E-01	3.65E+03	63.40
O5s	5	6.77E-01	2.24E+03	1482.07	2.95E-01	2.15E+03	52579.88	1.79E-01	-1.17E+03	73.31	-3.01E-01	8.33E+01	53.61	8.14E-04	1.94E+02	455.49	4.83E-02	2.91E+03	448.35
O6s	6	1.78E+00	3.22E+02	1393.23	-3.49E-01	3.31E+03	46301.86	9.90E-01	1.80E+02	63.43	-7.54E-01	3.78E+02	42.88	6.45E-01	3.59E+02	296.13	5.17E-01	2.96E+03	420.53
O7s	7	6.33E-01	1.07E+04	1871.91	7.13E-01	-5.73E+03	95173.13	1.69E+00	-5.47E+03	104.87	1.83E+00	-1.47E+03	110.39	2.12E+00	-1.72E+03	2305.31	1.48E+00	-1.10E+04	7688.06
O8s	8	-8.58E-01	7.80E+03	1739.43	1.79E+00	-6.56E+03	99651.85	4.50E-01	-3.06E+03	87.16	-9.66E-01	-1.66E+02	62.69	-7.75E-01	-5.17E+02	1142.15	1.14E+00	-9.37E+03	6848.34

	Minigraph						
	v(j)|h(q)|a(q)	*v(j)*	*h(q)*	*a(q)*	*v(j)*	*h(q)*	*a(q)*
Sample	**Distance**	**Ba**			**Pb**		
O1s	1	-1.35E+00	-8.89E+02	234.36	-1.66E-01	4.54E+02	33.66
O2s	2	-1.07E+00	-1.00E+03	213.60	-5.53E-01	4.28E+02	74.14
O3s	3	-6.72E-01	-1.25E+03	168.94	-7.13E-01	4.39E+02	57.50
O4s	4	-3.12E-01	4.53E+02	476.38	-3.71E-01	4.44E+02	48.46
O5s	5	1.91E-01	5.70E+02	497.63	6.23E-02	3.57E+02	183.07
O6s	6	1.02E+00	4.11E+02	468.81	7.02E-01	3.61E+02	176.34
O7s	7	1.06E+00	7.67E+02	532.99	2.10E+00	-2.05E+03	3890.81
O8s	8	1.13E+00	9.45E+02	565.16	-1.06E+00	-4.29E+02	1392.47

Global: 112	41 *36.6%*

A: Param.	**B: Cnt.**	**C: %**
Cu	1	7.10%
K	1	7.10%
Ca, Cr	2	14.30%
Ca, Cr, Mn, Fe,	6	42.90%
S, K, Ca, Ti, V,	12	85.70%
S, K, Ti, V, Mn,	12	85.70%
S, Ti, V, Fe, Ni,	7	50.00%

Source: Calculations made in TruVariogram software.

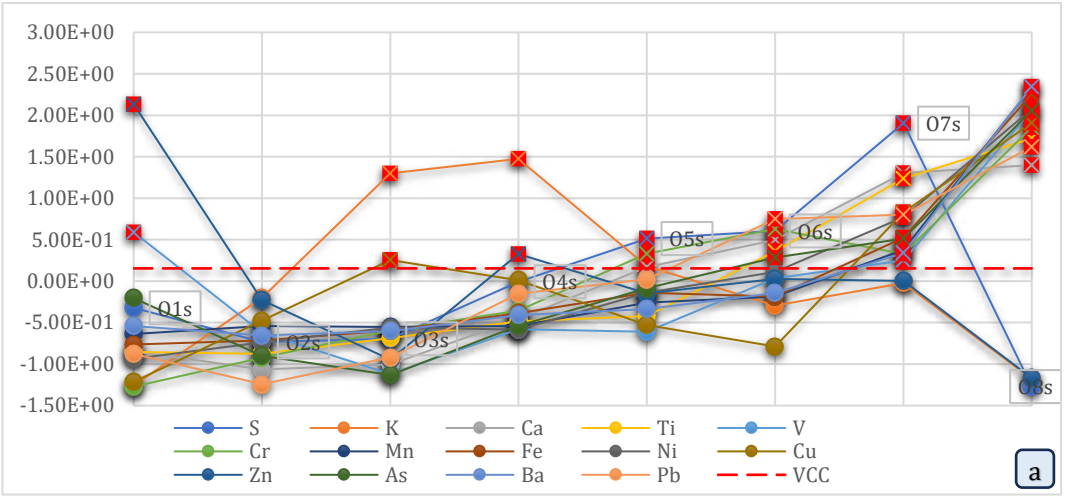

(a) Composite normalized variogram of surface sediments, 2021 campaign ($VCC_{Norm} = 0.154$).

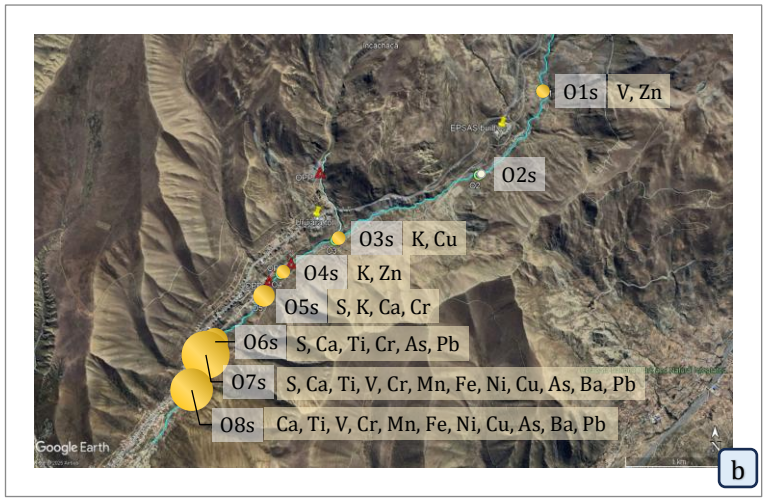

(b) Map of critical point evaluation, 2021 campaign.

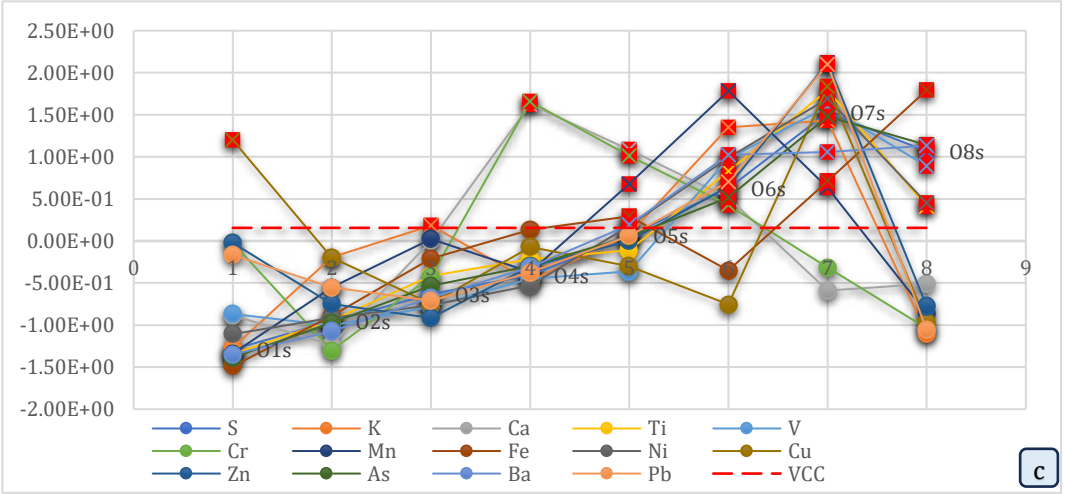

(c) Composite normalized variogram of surface sediments, 2024 campaign ($VCC_{Norm} = 0.156$).

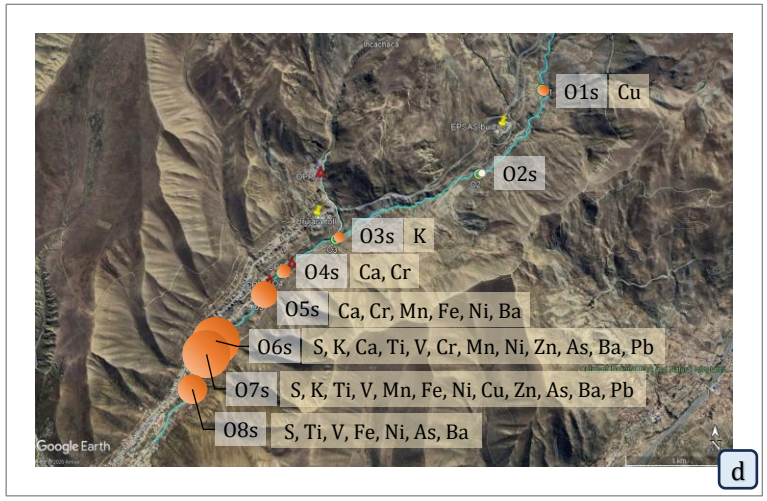

(d) Map of critical point evaluation, 2024 campaign.

The x-axis labels O1s–O8s indicate the sampling station associated with each normalized variance value $v(j)_{Norm}$ via the relationship $v(q) = v(j-1)$ (Equation 14). Red squares marked with an "X" indicate values exceeding VCC_{Norm}.

Figure 5. Composite normalized variograms and spatial distribution maps highlighting critical points in surface sediment samples from the Orckojahuira River segment influenced by mineral processing plants.

Source: Authors' own elaboration based on TruVariogram software. Satellite images from Google Earth, 2025.

Table 7. As Table 5, for deep sediment samples (5–15 cm) from the 2021 campaign (1st campaign). A VCC_{Norm} of 0.155 was applied.

		Minigraph																
	v(j)/h(q)/a(q)	*v(j)*	*h(q)*	*a(q)*	*v(j)*	*h(q)*	*a(q)*	*v(j)*	*h(q)*	*a(q)*	*v(j)*	*h(q)*	*a(q)*	*v(j)*	*h(q)*	*a(q)*	*v(j)*	*h(q)*	*a(q)*
Sample	**Distance**	**S**			**K**			**Ca**			**Ti**			**V**			**Cr**		
O1p	1	-1.34E+00	1.88E+02	5340.14	-1.29E+00	7.99E+01	29079.50	-1.47E+00	-1.33E+03	7106.17	-1.54E+00	1.20E+03	5505.64	-5.51E-01	8.07E+02	249.67	8.55E-01	-1.02E+02	90.83
O2p	2	-7.99E-01	1.66E+03	1577.78	4.41E-01	-2.74E+03	25834.38	-7.29E-01	-8.18E+03	1361.69	-5.92E-01	4.20E+02	5310.22	-5.47E-01	3.83E+01	181.54	-5.26E-01	-1.03E+03	113.29
O3p	3	-6.04E-01	1.69E+03	1479.32	6.87E-01	2.93E+02	29324.89	-4.86E-01	-7.79E+03	1691.43	-1.26E-01	3.02E+03	5964.33	-5.84E-01	2.41E+02	199.49	-7.74E-01	-1.09E+02	91.01
O4p	4	-5.95E-01	1.61E+03	1690.67	1.70E-03	-1.18E+03	27633.07	-6.41E-01	-7.67E+03	1790.00	-7.54E-01	1.48E+03	5578.32	-5.10E-01	-1.85E+01	176.52	1.93E-01	1.36E+02	85.08
O5p	5	1.70E-01	-9.17E+02	8172.80	1.48E+00	3.06E+02	29339.96	2.33E-01	7.85E+03	14792.99	6.60E-01	-2.38E+03	4604.22	-2.01E-01	-2.96E+02	151.93	1.50E-01	4.63E+02	77.17
O6p	6	5.19E-01	4.99E+01	5695.19	6.49E-01	3.73E+03	33287.07	5.16E-01	-2.27E+03	6319.95	7.90E-01	2.82E+02	5275.45	3.36E-02	-1.56E+02	164.36	1.27E+00	1.49E+02	84.75
O7p	7	1.19E+00	-1.62E+02	6239.49	-7.52E-01	1.25E+02	29131.88	1.22E+00	2.08E+03	9958.55	-4.99E-02	-1.03E+03	4945.65	-3.97E-02	5.18E+01	182.74	6.51E-01	5.52E+02	75.00
O8p	8	1.46E+00	-4.12E+03	16389.39	-1.22E+00	-6.24E+02	28268.48	1.36E+00	1.73E+04	22730.01	1.62E+00	-2.99E+03	4450.69	2.40E+00	-6.68E+02	118.97	-1.82E+00	-5.96E+01	89.81

		Minigraph																
	v(j)/h(q)/a(q)	*v(j)*	*h(q)*	*a(q)*	*v(j)*	*h(q)*	*a(q)*	*v(j)*	*h(q)*	*a(q)*	*v(j)*	*h(q)*	*a(q)*	*v(j)*	*h(q)*	*a(q)*	*v(j)*	*h(q)*	*a(q)*
Sample	**Distance**	**Mn**			**Fe**			**Ni**			**Cu**			**Zn**			**As**		
O1p	1	-6.54E-01	4.36E+02	477.08	-7.26E-01	1.60E+03	62993.25	-7.11E-01	1.23E+03	0.00	-1.03E+00	5.96E+02	54.48	-1.22E+00	2.04E+03	721.79	-5.96E-01	1.57E+02	91.13
O2p	2	-5.04E-01	5.59E+02	431.17	-7.49E-01	-2.44E+02	28009.00	-4.99E-01	-2.82E+02	81.82	4.10E-01	-6.69E+02	34.96	-6.09E-01	-3.52E+02	214.81	-9.56E-01	4.43E+02	41.04
O3p	3	-6.81E-02	-1.86E+01	646.31	-6.57E-01	-2.48E+02	27932.24	-3.43E-01	-3.67E+02	86.43	1.46E+00	-7.58E+02	33.59	-5.41E-01	5.37E+01	300.67	-9.98E-01	4.25E+02	44.31
O4p	4	-1.22E-01	-6.12E+02	867.20	-4.79E-01	-2.90E+02	27134.42	-3.76E-01	-1.53E+02	74.85	4.70E-01	-3.59E+01	44.73	-7.39E-01	5.45E+02	404.69	-4.95E-01	4.47E+02	40.37
O5p	5	-9.65E-01	7.81E+01	610.24	-3.26E-01	-2.27E+02	28325.77	-3.63E-01	-3.02E+01	68.17	-9.30E-01	8.71E+02	58.71	3.46E-02	-6.94E+02	142.48	-2.17E-02	2.13E+02	81.29
O6p	6	-5.70E-01	3.48E+02	509.71	-4.54E-02	-1.88E+02	29061.16	-2.18E-01	-3.45E+01	68.41	9.10E-01	-3.30E+02	40.18	3.63E-01	-7.76E+02	125.21	2.58E-01	-2.91E+02	169.69
O7p	7	7.75E-01	3.09E+02	524.23	9.00E-01	-3.21E+02	26533.97	1.04E-01	-2.54E+01	67.91	1.77E-02	9.47E+01	46.74	8.51E-01	-6.00E+02	162.39	9.14E-01	8.68E+00	117.15
O8p	8	2.11E+00	-1.10E+03	1048.92	2.08E+00	-8.27E+01	31061.27	2.41E+00	-3.35E+02	84.69	-1.31E+00	2.31E+02	48.85	1.86E+00	-2.21E+02	242.54	1.89E+00	-1.40E+03	364.41

		Minigraph					
	v(j)/h(q)/a(q)	*v(j)*	*h(q)*	*a(q)*	*v(j)*	*h(q)*	*a(q)*
Sample	**Distance**	**Ba**			**Pb**		
O1p	1	-1.49E+00	1.46E+03	2048.55	-5.20E-01	3.01E+01	67.83
O2p	2	4.73E-01	-5.94E+02	2151.32	-1.27E+00	6.91E+02	40.57
O3p	3	1.48E+00	-4.21E+03	2331.91	-1.28E+00	5.72E+02	45.45
O4p	4	-6.23E-01	-2.06E+03	2224.62	-2.73E-01	4.98E+02	48.52
O5p	5	-4.89E-02	4.71E+03	1886.15	3.60E-01	4.25E+02	51.54
O6p	6	1.14E+00	-2.23E+03	2232.91	6.16E-01	-6.34E+02	95.24
O7p	7	-1.12E-01	-1.16E+03	2179.76	1.34E+00	-2.23E+02	78.30
O8p	8	-8.21E-01	4.08E+03	1917.85	1.03E+00	-1.36E+03	125.17

Global: 112	42 *37.5%*

A: Param.	**B: Cnt.**	**C: %**
Cr	1	7.10%
K, Cu, Ba	3	21.40%
K, Cu, Ba	3	21.40%
Cr, Cu	2	14.30%
S, K, Ca, Ti, Pb	5	35.70%
S, K, Ca, Ti, Cr, Cu, Zn, As, Ba, Pb	10	71.40%
S, Ca, Cr, Mn, Fe, Zn, As, Pb	8	57.10%
S, Ca, Ti, V, Mn, Fe, Ni, Zn, As, Pb	10	71.40%

Source: Calculations made in TruVariogram software.

Table 8. As Table 5, for deep sediment samples (5–15 cm) from the 2024 campaign (2nd campaign). A VCC_{Norm} of 0.156 was applied.

	Minigraph																		
	v(j)/h(q)/a(q)	*v(j)*	*h(q)*	*a(q)*	*v(j)*	*h(q)*	*a(q)*	*v(j)*	*h(q)*	*a(q)*	*v(j)*	*h(q)*	*a(q)*	*v(j)*	*h(q)*	*a(q)*	*v(j)*	*h(q)*	*a(q)*
Sample	**Distance**	**S**			**K**			**Ca**			**Ti**			**V**			**Cr**		
O1p	1	-1.17E+00	-2.74E+03	503.05	-9.21E-01	-2.47E+02	25879.82	-1.49E+00	-7.30E+02	4715.60	-1.04E+00	2.10E+03	6000.66	-1.22E+00	-1.58E+04	126.67	-1.54E+00	-7.44E+02	79.94
O2p	2	-9.54E-01	-2.71E+03	678.89	-1.26E+00	1.33E+03	31464.17	-1.17E+00	-7.92E+02	3467.29	-9.51E-01	4.95E+03	7289.48	-8.85E-01	-7.60E+04	176.21	-9.79E-01	-2.30E+03	97.64
O3p	3	-6.15E-01	-2.72E+03	622.46	-9.36E-01	6.95E+02	29213.68	-5.59E-01	-7.64E+02	4033.62	-7.53E-01	1.90E+03	5912.84	-5.59E-01	-5.33E+04	157.58	-4.92E-02	-2.31E+03	97.78
O4p	4	-4.38E-01	-2.32E+03	3230.52	3.34E-02	1.49E+03	32011.04	9.66E-02	-2.13E+01	18914.91	-4.70E-01	4.58E+02	5259.58	-4.80E-01	4.49E+03	110.00	6.09E-01	4.20E+02	66.65
O5p	5	-1.85E-02	-7.63E+02	13233.37	6.13E-01	1.66E+02	27342.92	6.97E-01	7.47E+02	34325.01	-5.99E-03	-2.19E+02	4953.66	8.09E-02	9.29E+02	112.93	1.01E+00	1.48E+03	54.53
O6p	6	4.02E-01	-1.41E+03	9082.98	8.56E-01	1.54E+02	27297.81	1.09E+00	9.83E+02	39050.21	9.34E-01	-7.29E+02	4723.18	1.23E+00	3.93E+03	110.46	1.26E+00	1.83E+03	50.61
O7p	7	1.16E+00	5.42E+03	53058.45	1.61E+00	-1.42E+03	21739.67	1.71E-01	-5.82E+01	18175.00	1.76E+00	-4.59E+03	2979.84	1.62E+00	6.74E+04	58.26	4.17E-01	7.66E+02	62.71
O8p	8	1.63E+00	7.24E+03	64785.79	7.48E-03	-2.17E+03	19089.21	1.17E+00	6.34E+02	32055.08	5.24E-01	-3.88E+03	3301.01	2.24E-01	6.83E+04	57.46	-7.19E-01	8.53E+02	61.72

	Minigraph																		
	v(j)/h(q)/a(q)	*v(j)*	*h(q)*	*a(q)*	*v(j)*	*h(q)*	*a(q)*	*v(j)*	*h(q)*	*a(q)*	*v(j)*	*h(q)*	*a(q)*	*v(j)*	*h(q)*	*a(q)*	*v(j)*	*h(q)*	*a(q)*
Sample	**Distance**	**Mn**			**Fe**			**Ni**			**Cu**			**Zn**			**As**		
O1p	1	-1.27E+00	8.30E+01	1359.66	-1.05E+00	-7.96E+02	44125.33	-1.06E+00	1.76E+03	36.49	-1.06E+00	1.45E+03	38.76	-1.00E+00	-7.09E+02	137.83	-1.08E+00	-7.41E+02	20.67
O2p	2	-1.01E+00	-1.50E+03	736.82	-8.16E-01	-3.85E+02	58328.31	-8.98E-01	1.18E+03	45.54	-1.03E+00	6.36E+02	57.51	-8.12E-01	-6.02E+02	235.60	-8.81E-01	-7.28E+02	70.29
O3p	3	-7.49E-01	-1.56E+03	713.00	-4.64E-01	-5.13E+02	53906.96	-8.91E-01	1.08E+03	47.11	-6.57E-01	4.55E+02	61.71	-4.95E-01	-5.02E+02	326.42	-5.12E-01	-7.32E+02	52.95
O4p	4	-4.23E-01	-1.15E+03	873.29	-3.52E-01	-9.32E+02	39429.32	-4.60E-01	1.89E+03	34.48	-1.77E-01	1.73E+03	32.10	-4.17E-01	-4.40E+02	382.60	-4.04E-01	-7.12E+02	126.48
O5p	5	2.80E-01	2.41E+02	1421.79	-4.39E-02	-4.38E+02	56512.24	6.83E-01	-2.05E+03	95.52	-2.42E-02	7.23E+02	55.50	-2.20E-01	-3.56E+02	460.04	-1.25E-01	-4.56E+02	1054.34
O6p	6	8.45E-01	4.18E+02	1491.65	3.92E-03	-6.33E+02	49772.42	5.41E-02	-3.04E+02	68.46	4.20E-02	6.64E+02	56.87	1.00E-01	-4.67E+02	358.80	2.01E-01	-6.08E+02	502.08
O7p	7	1.39E+00	4.29E+02	1496.22	5.81E-01	9.43E+02	#######	8.89E-01	-1.59E+03	88.35	1.72E+00	-3.43E+03	151.59	7.85E-01	7.62E+02	1480.01	8.40E-01	1.13E+03	6776.65
O8p	8	9.42E-01	3.03E+03	2523.05	2.14E+00	2.75E+03	#######	1.68E+00	-1.96E+03	94.11	1.18E+00	-2.23E+03	123.85	2.06E+00	2.31E+03	2894.20	1.96E+00	2.85E+03	13026.20

	Minigraph									
	v(j)/h(q)/a(q)	*v(j)*	*h(q)*	*a(q)*	*v(j)*	*h(q)*	*a(q)*			
Sample	**Distance**	**Ba**			**Pb**			**A: Param.**	**B: Cnt.**	**C: %**
O1p	1	-1.31E+00	-1.89E+03	72.01	-1.16E+00	-1.43E+03	33.32			
O2p	2	-7.02E-01	-3.03E+02	325.90	-9.28E-01	-1.38E+03	58.45			
O3p	3	-3.71E-01	-9.84E+01	358.75	-5.21E-01	-1.39E+03	53.05			
O4p	4	-6.18E-01	-6.86E+02	264.64	-4.04E-01	-1.36E+03	67.64	Cr	1	7.10%
O5p	5	4.72E-01	1.09E+03	548.75	-8.03E-02	-7.88E+02	362.96	K, Ca, Cr, Mn, Ni, Ba	6	42.90%
O6p	6	6.37E-01	1.27E+03	578.67	2.76E-01	-1.23E+03	135.19	S, K, Ca, Ti, V, Cr, Mn, As, Ba, Pb	10	71.40%
O7p	7	-2.44E-02	9.50E+01	389.74	1.00E+00	2.80E+03	2213.06	S, K, Ca, Ti, V, Cr, Mn, Fe, Ni, Cu, Zn, As, Pb	13	92.90%
O8p	8	1.91E+00	5.19E+02	457.71	1.81E+00	4.78E+03	3229.60	S, Ca, Ti, V, Mn, Fe, Ni, Cu, Zn, As, Ba, Pb	12	85.70%

Global: 112 | 42 | *37.5%*

Source: Calculations made in TruVariogram software.

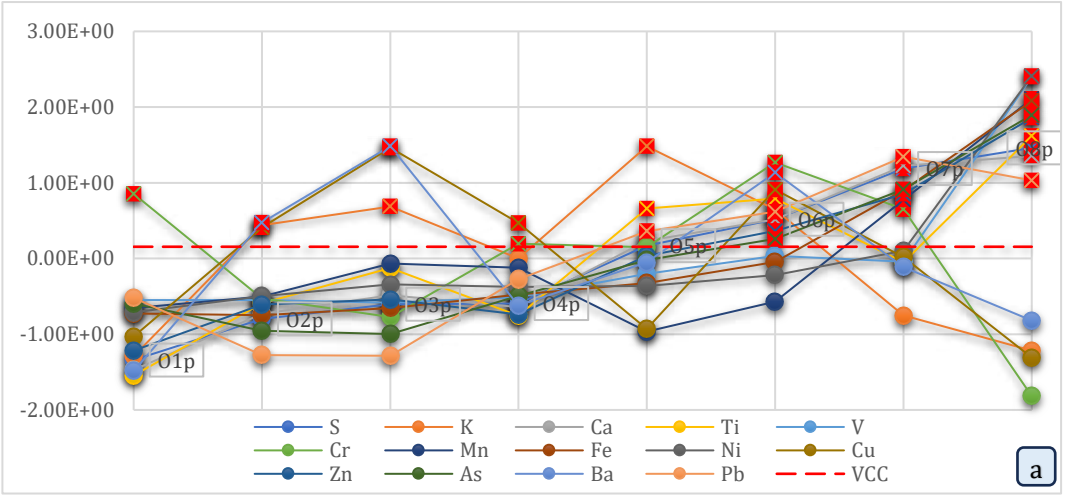

(a) Composite normalized variogram of deep sediments, 2021 campaign ($VCC_{Norm} = 0.155$).

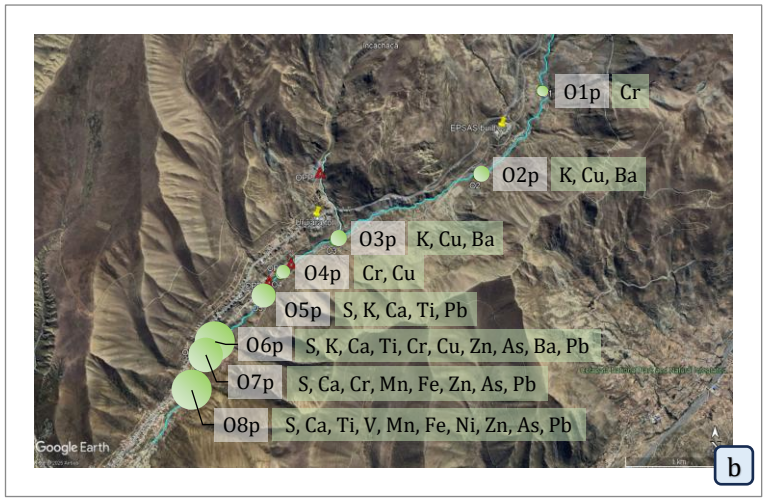

(b) Map of critical point evaluation, 2021 campaign.

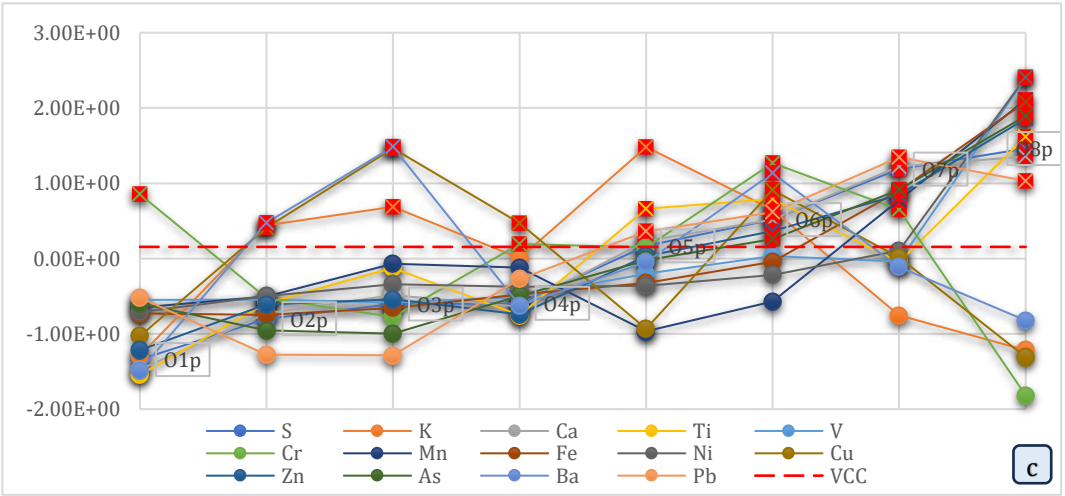

(c) Composite normalized variogram of deep sediments, 2024 campaign ($VCC_{Norm} = 0.156$).

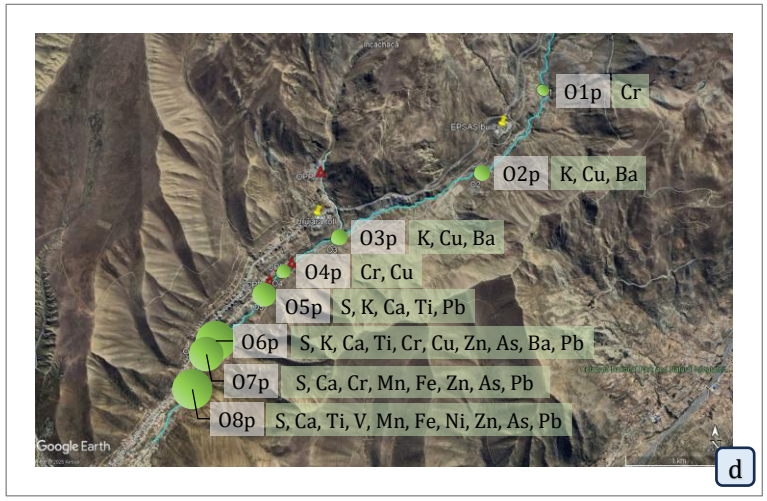

(d) Map of critical point evaluation, 2024 campaign.

The x-axis labels O1s–O8s indicate the sampling station associated with each normalized variance value $v(j)_{Norm}$ via the relationship $v(q) = v(j-1)$ (Equation 14). Red squares marked with an "X" indicate values exceeding VCC_{Norm}.

Figure 6. As Figure 5, for deep sediment samples (5–15 cm). $VCC_{Norm} = 0.155$ (2021 campaign) and 0.156 (2024 campaign).

Source: Authors' own elaboration based on TruVariogram software. Satellite images from Google Earth, 2025.

Results as a summary

The methodology was applied to four independent case studies of contaminated river systems —Tamla Nala (India), Warta (Poland), Elbe (Germany), and Orckojahuira (Bolivia)— using published concentration data for the first three cases and original XRF sediment data for the fourth. In all cases, the VCC_{Norm} criterion was applied exclusively, with threshold values derived from the empirical estimator (Equation 7) for each composite normalized variogram. The key findings are summarized below in Table 9.

For the Tamla Nala stream, the analysis identified 39.3% critical parameter-point regarding anions/BOD/COD and 41.7% in cations, across 128 total evaluations (16 parameters × 8 stations), using VCC_{Norm} values of 0.158 for the anion/BOD/COD group and 0.154 for the cation group. The spatial distribution exhibits a clear downstream gradient: stations S1 and S2 show no or minimal critical parameters, while S6 reaches 14 of 16 parameters critical (87.5%), coinciding with the highest density of steel, chemical, and pharmaceutical facilities identified along the watercourse. All ten contaminants highlighted by the researchers (Pobi et al., 2019) as most concerning —CN^-, Hg, Pb, Fe, Cr, Cd, Cu, Ni, COD, and Cl^-— are flagged as critical in at least three stations, confirming full agreement with the original authors' conclusions. An additional finding is the identification of NO_3^- variability at S2, S3, and S6, attributable to mixed domestic and agricultural sources not addressed by the original industrial-focused assessment.

For the Warta River, the analysis evaluated 144 parameter-point combinations (6 parameters × 24 stations) for each of two years. In 2016, 39 combinations were critical (27.1%, $VCC_{Norm} = 0.215$); in 2017, 43 were critical (29.9%, $VCC_{Norm} = 0.204$). The slight increase from 2016 to 2017 —despite an overall reduction in mean metal concentrations documented by the authors (Jaskuła et al., 2021)— reflects a broader spatial spread of cadmium and copper contamination rather than intensification at specific points. The lower course from p18 onward remains the most impacted zone in both years, consistent with the cluster analysis results of the original authors, while the city of Konin near p14–p15 emerges as a secondary contamination source detectable in both campaigns.

For the Elbe River, the analysis evaluated 27 parameter-point combinations (3 TOC-normalized parameters × 9 stations) following the 2002 flood, applying a VCC_{Norm} of 0.173. Fourteen combinations were identified as critical (51.9%). The spatial pattern fully reproduces the contamination narrative described in the study (Brack et al., 2008): KON and DRE are non-critical, consistent with their role as upstream reference stations; TOR through MAG flag all three compound classes (PCDD/F, PCNs, and PCBs) as critical, reflecting the downstream mobilization of industrial contaminants from the Bitterfeld zone; ARN is non-critical, confirming the documented recovery boundary; and HIT flags only PCBs, consistent with the diffuse multi-source PCB pattern reported by the original authors.

For the Orckojahuira River, four datasets were evaluated across two campaigns and two sediment depths (14 parameters × 8 stations = 112 combinations each), using VCC_{Norm} values of 0.154–0.156. Critical parameter proportions are 34.8% and 36.6% for surface sediments in 2021 and 2024 respectively, and 37.5% in both years for deep sediments. The modest but consistent increase between campaigns in surface sediments reflects escalating mining pressure on the studied segment, corroborated by the pronounced rise in lead concentrations at the downstream stations O7 and O8 between 2021 and 2024. In deep sediments, station O7 in the 2024 campaign reaches 13 of 14 critical parameters (92.9%), the highest value across all datasets in this study. The variographic results are in complete agreement with the field-based classification presented in Table 4, validating the methodology's ability to reproduce expert judgment from quantitative variogram data alone.

Table 9. Summary of VCC_{Norm}-based critical point evaluation across the four case studies. VCC_{Norm} values were derived using Equation 7 applied parameter by parameter and summarized as the median across all parameters in each composite variogram.

Total combinations = number of parameters × number of sampling stations.

Case study	Dataset	VCC_{Norm} (Eq. 7, average)	Total combinations	Critical	%
Tamla Nala	Water (anions/BOD/COD)	0.158	56	22	39.3%
Tamla Nala	Water (cations)	0.154	72	30	41.7%
Warta	Sediments 2016	0.215	144	39	27.1%
Warta	Sediments 2017	0.204	144	43	29.9%
Elbe	Sediments (TOC)	0.173	27	14	51.9%
Orckojahuira	Surface 2021	0.154	112	39	34.8%
Orckojahuira	Surface 2024	0.156	112	41	36.6%
Orckojahuira	Deep 2021	0.155	112	42	37.5%
Orckojahuira	Deep 2024	0.156	112	42	37.5%

Across all four case studies, the conclusions drawn from the VCC_{Norm}-based evaluation are consistent with those of the original investigators, who employed pollution indices, enrichment factors, cluster analysis, bioassays, and direct field observation. This concordance —achieved without recourse to external regulatory thresholds or source attribution models— demonstrates the versatility and transferability of the methodology across different environmental matrices, contaminant classes, geographical contexts, and data origins. The VCC_{Norm} values across all datasets fall within a narrow range (0.154–0.215), confirming the adaptive behavior of the empirical estimator and its consistent scaling with the statistical structure of each variogram.

Conclusions

This study introduces a methodology for the identification of critical sampling points in river monitoring systems, grounded in the one-dimensional heterogeneity variography formalized by Pierre Gy and extended here to environmental assessment contexts. The central contribution is the Value for Critical Comparisons (VCC_{Norm}), an adaptive threshold derived empirically from the statistical structure of each composite normalized variogram (Equation 7), which scales automatically with the magnitude and dispersion of the dataset and requires no reference to external regulatory standards. This property makes the methodology applicable across diverse environmental matrices, contaminant classes, and geographical contexts —including data-scarce or regulation-deficient settings where conventional index-based approaches may be unavailable or contested.

The practical efficacy of the methodology is substantiated through four independent case studies. For the Tamla Nala stream (India), the VCC_{Norm}-based evaluation identified 40.6% of parameter-point combinations as critical, in full agreement with the conclusions of Pobi et al. (2019) regarding the dominant influence of industrial discharges on water quality, while additionally flagging nitrate variability attributable to diffuse domestic sources not addressed in the original study. For the Warta River (Poland), the methodology reproduced the spatial contamination gradient documented by Jaskuła et al. (2021) —with the lower course consistently identified as the most impacted zone— and revealed that a slight increase in the percentage of critical combinations from 2016 (27.1%) to 2017 (29.9%) reflects a broader spatial spread of cadmium and copper rather than an overall intensification, a nuance not captured by global pollution indices. For the Elbe River (Germany), a VCC_{Norm} of 0.173 reproduced the full spatial narrative of post-flood PCN, PCDD/F, and PCB contamination described by Brack et al. (2008), correctly identifying Königstein and Dresden as non-critical upstream reference stations, the Torgau–Magdeburg corridor as the most impacted zone, and Arneburg as the recovery boundary —without recourse to Toxic Equivalent Quotient thresholds or bioassay data.

A particularly compelling validation was obtained by the author or this article in the Orckojahuira River segment (Bolivia), where direct field access permitted comparison between variographic outputs and expert professional judgment. The methodology identified stations O3 through O8 as critical in all four datasets evaluated (surface and deep sediments, 2021 and 2024 campaigns), in complete agreement with field observations of mining tailings discharge. The pronounced increase in lead concentrations at stations O7 and O8 between campaigns —from approximately 80–120 $mg{\cdot}kg^{-1}$ in 2021 to over 2 200–3 200 $mg{\cdot}kg^{-1}$ in 2024 in deep sediments— was correctly identified as a critical escalation, supporting the hypothesis of intensified galena-rich tailings discharges and demonstrating the methodology's capacity to detect temporal trends across repeated campaigns.

Across all four case studies, the VCC_{Norm} values derived from Equation 7 fall within a narrow range (≈0.15–0.22), confirming the adaptive and consistent behavior of the empirical estimator regardless of the environmental matrix, number of parameters, or geographic context. This consistency is a methodological result in its own right: it demonstrates that the statistical structure of heterogeneity variograms from contaminated river systems shares a common scaling behavior, which the estimator captures reliably.

The stochastic nature of anthropogenic contamination —shaped by episodic events such as floods, dam breaches, and variable industrial discharge— makes spatial identification of critical points inherently more informative than system-wide averages. The variographic approach excels precisely in this context, capturing spatial and temporal dependencies that traditional statistical summaries obscure. Future monitoring campaigns at the sites studied here should prioritize the critical zones identified: the whole Tamla Nala stream in India with emphasis in BOD, COD, nitrate, cyanide and mercury; the lower Warta River in Polland from station p18 onward; the Torgau–Magdeburg corridor in the Elbe in Germany; and the full O3–O8 segment of the Orckojahuira River, where additional downstream sampling stations are recommended to characterize the extent of contamination before its confluence with the urban Choqueyapu River system in Bolivia.

The proposed methodology does not supplant existing techniques based on contamination indices, enrichment factors, or multivariate cluster analysis. It serves as a complementary, threshold-independent evaluation tool that operates at the individual sampling point level, identifying which parameters and locations warrant further investigation without requiring control samples or regulated reference values. To support practical

implementation, a VBA-Excel™ application named TruVariogram has been developed, streamlining variogram construction, VCC_{Norm} estimation, and results visualization through ChartMaps —a novel chart type that integrates georeferenced sampling point maps with critical parameter outputs, supporting informed decision-making in environmental management.

Declaration of funding

No funding was received for this research.

Ethical responsibilities of authors

All authors have read, understood, and have complied as applicable with the statement on Ethical responsibilities of Authors as found in the Instructions for Authors.

Ethics approval and consent to participate

Not applicable. This study does not involve human participants, human data, human tissue, animals, or client-owned animals.

Data availability statement

The datasets generated and analyzed during the current study are available from the corresponding author on reasonable request. The TruVariogram application is available upon request to the corresponding author.

References

AAPS - PERIAGUA III. (2022). *Indicadores de desempeño de las EPSA en Bolivia-gestión 2022* (No. 6972). AAPS - PERIAGUA III. https://www.bivica.org/file/view/id/6972

Alshahrani, M. A., Ahmad, M., Laiq, M., & Nabi, M. (2025). Geostatistical analysis and multivariate assessment of groundwater quality. *Scientific Reports*, *15*(1), 7435. https://doi.org/10.1038/s41598-025-91055-3

Arze Landivar, C., Romero Prieto, C., & Velasco Quintanilla, F. (2025). *Química Analítica y el Equilibrio Químico*. McGraw-Hill. https://www.mheducation.com.mx/quimica-analitica-y-equilibrio-quimico-9786071522320-latam-group

Brack, W., Bláha, L., Giesy, J. P., Grote, M., Monika, M., Schrader, S., & Hecker, M. (2008). Polychlorinated naphthalenes and other dioxin-like compounds in Elbe River sediments. *Environmental Toxicology and Chemistry*, *27*(3). https://doi.org/doi.org/10.1897/07-400.1

de Alves, M. C., da Silva, F. M., Moraes, J. C., Pozza, E. A., de Oliveira, M. S., Souza, J. C. S., & Alves, L. S. (2011). Geostatistical analysis of the spatial variation of the berry borer and leaf miner in a coffee agroecosystem. *Precision Agriculture*, *12*(1), 18–31. https://doi.org/10.1007/s11119-009-9151-z

Fortuna, A., Steiner, J. L., Moriasi, D. N., Northup, B. K., & Starks, P. J. (2022). Linking geospatial information and effects of land management to edaphic properties. *Journal of Soil and Water Conservation*, *77*(1), 45–58. https://doi.org/10.2489/jswc.2022.00160

Gordon, L. M., Bennett, S. J., Wells, R. R., & Alonso, C. V. (2007). Effect of soil stratification on the development and migration of headcuts in upland concentrated flows. *Water Resources Research*, *43*(7). https://doi.org/10.1029/2006WR005659

Gy, P. (Ed.). (1992a). *Sampling of heterogeneous and dynamic material systems: Theories of heterogeneity, sampling, and homogenizing*. Elsevier.

Gy, P. (1992b). *Sampling of particulate materials: Theory and practice* (2. rev. ed., 3. printing). Elsevier Scientific.

Hoang, H. A., Vu, T. D., & Nguyen, T. T. (2017). Spatial Variability Analysis of Cu Content: A Case Study in Jiurui Copper Mining Area. *International Journal of Applied Geospatial Research (IJAGR)*, *8*(1), 81–93. https://doi.org/10.4018/IJAGR.2017010105

Huallpara Lliully, L., García Moreno, M. E., Villca, A., & Ormachea Muñoz, M. R. [supervisores. (2010). *Inspección y monitoreo ambiental de los principales ríos del Municipio de La Paz* [Thesis, Universidad Mayor de San Andres. Facultad de Ciencias Puras y Naturales. Carrera Ciencias Químicas]. https://repositorio.umsa.bo/xmlui/handle/123456789/17958

Ibañez Apaza, L. I. (2022). *Balance hídrico de la cuenca del Río La Paz hasta el punto de control Estación Hidrométrica de Aranjuez* [Thesis]. https://repositorio.umsa.bo/xmlui/handle/123456789/32319

Jaskuła, J., Sojka, M., Fiedler, M., & Wróżyński, R. (2021). Analysis of Spatial Variability of River Bottom Sediment Pollution with Heavy Metals and Assessment of Potential Ecological Hazard for the Warta River, Poland. *Minerals*, *11*(3), Article 3. https://doi.org/10.3390/min11030327

Liberman, M., Soliz, H., Mercado, M., Zeballos, M., Martinez, O., & Rocabado, P. (2021). *Línea base e indicadores para el monitoreo de la biodiversidad y fuentes de agua en el Municipio de La Paz*. Gobierno Autónomo Municipal de La Paz - GAMLP. https://sitservicios.lapaz.bo/biodiversidad/

Matheron, G. (1965). *Les variables régionalisées et leur estimation: Une application de la théorie de fonctions aléatoires aux sciences de la nature*. Masson et Cie.

Mayer, B. (2025). Climate Effects in Environmental Impact Assessment. *Transnational Environmental Law*, *14*(2), 342–364. https://doi.org/10.1017/S2047102524000402

Minnitt, R., & Esbensen, K. (2017). Pierre Gy's development of the Theory of Sampling: A retrospective summary with a didactic tutorial onquantitative sampling of one-dimensional lots. *TOS Forum*, *2013*(1), 7. https://doi.org/10.1255/tosf.96

Onyango, C. M., Nyaga, J. M., Wetterlind, J., Söderström, M., & Piikki, K. (2021). Precision Agriculture for Resource Use Efficiency in Smallholder Farming Systems in Sub-Saharan Africa: A Systematic Review. *Sustainability*, *13*(3), 1158. https://doi.org/10.3390/su13031158

Pobi, K. K., Satpati, S., Subhajit Dutta, Dutta, S., Sumanta Nayek, Rajnarayan Saha, Saha, R., & Gupta, S. (2019). Sources evaluation and ecological risk assessment of heavy metals accumulated within a natural stream of Durgapur industrial zone, India, by using multivariate analysis and pollution indices. *Applied Water Science*, *9*(3), 1–16. https://doi.org/10.1007/s13201-019-0946-4

Roberts, N. J. (2016, April 20). *Late Cenozoic geology of La Paz, Bolivia, and its relation to landslide activity*. Simon Fraser University. https://summit.sfu.ca/item/16449

Romero Prieto, C., & Guzmán Alegria, L. (2024). Confidence and Prediction Bands in Linear and Nonlinear Chemometric Regression Models. *Analytical Letters*, *57*(12), 1841–1860. https://doi.org/10.1080/00032719.2023.2278662

Teegavarapu, R. S. V. (2007). Use of universal function approximation in variance-dependent surface interpolation method: An application in hydrology. *Journal of Hydrology*, *332*(1–2), 16–29. https://doi.org/10.1016/j.jhydrol.2006.06.017

Webster, R., & Oliver, M. A. (2007). *Geostatistics for environmental scientists* (2nd ed). John Wiley & sons.

Supplementary Information

One-dimensional heterogeneity variography for critical point identification in environmental monitoring: a methodology based on Gy's sampling theory

Table s.1. Results of the variography evaluation and the proposed methodology based on the data in Table s.**2** and Table s.**3**. Evaluation is made with a total of 144 points (6 parameters times 24 sample points).

	2016	Global: 144	39 *27.1%*	2017	Global: 144	43 *29.9%*
Muestra	**A: Param.**	**B: Qty.**	**C: %**	**A: Param.**	**B: Qty.**	**C: %**
p1	Ni, Pb, Zn	3	50.00%			
p2						
p3						
p4						
p5				Cd	1	16.70%
p6						
p7						
p8	Zn	1	16.70%			
p9						
p10				Cd, Cu	2	33.30%
p11				Cd, Cu	2	33.30%
p12				Cd, Cu	2	33.30%
p13	Zn	1	16.70%	Cd, Cu, Zn	3	50.00%
p14				Cd, Cu, Zn	3	50.00%
p15	Cu, Pb, Zn	3	50.00%	Cd, Cu	2	33.30%
p16	Cu	1	16.70%	Cd, Zn	2	33.30%
p17	Cu, Pb	2	33.30%	Cd, Cu	2	33.30%
p18	Cd, Cr, Cu, Pb, Zn	5	83.30%	Cd, Cu, Pb	3	50.00%
p19	Cd, Cu, Ni, Pb, Zn	5	83.30%	Cd, Cu, Ni, Pb	4	66.70%
p20	Cd	1	16.70%			
p21	Cd, Cr, Cu, Ni, Pb, Zn	6	100.00%	Cr, Ni, Pb, Zn	4	66.70%
p22	Cd, Cr, Cu, Ni, Pb	5	83.30%	Cr, Cu, Ni, Pb, Zn	5	83.30%
p23	Cd, Cu, Pb, Zn	4	66.70%	Cr, Cu, Pb, Zn	4	66.70%
p24	Cr, Ni	2	33.30%	Cr, Cu, Ni, Zn	4	66.70%

Source: Calculations made in TruVariogram software.

Table s.2. Calculated normalized variance values $v(j)_{Norm}$ and critical point evaluation for the Warta River, Poland, based on data reported by Jaskuła et al. (2021). A VCC_{Norm} of 0.215 was applied to the 2016 dataset. The evaluation comprises 144 parameter-point combinations (6 parameters × 24 sample collection stations) for 2016.

	Minigraph																		
	v(q)|h(q)|a(q)	*v(q)*	*h(q)*	*a(q)*	*v(q)*	*h(q)*	*a(q)*	*v(q)*	*h(q)*	*a(q)*	*v(q)*	*h(q)*	*a(q)*	*v(q)*	*h(q)*	*a(q)*	*v(q)*	*h(q)*	*a(q)*
Sample	**Distance**	**Cd**			**Cr**			**Cu**			**Ni**			**Pb**			**Zn**		
p1	1	-4.30E-01	-7.17E+02	0.37	-1.38E-02	1.81E+03	193.00	-5.92E-01	3.46E+01	23.20	1.72E+00	4.72E+02	22.20	6.03E-01	-1.52E+02	27.00	5.92E-01	4.95E+02	168.00
p2	2	-3.58E-01	-6.27E+02	0.52	-2.59E-01	-6.26E+02	4.32	-3.61E-01	-8.22E+02	0.40	9.23E-02	-1.01E+03	2.84	-7.23E-02	-6.69E+02	12.00	-1.57E-02	1.03E+03	200.00
p3	3	-6.52E-01	-8.60E+02	0.13	-5.61E-01	-4.57E+02	17.40	-8.24E-01	-8.22E+02	0.40	-8.58E-01	-4.36E+02	10.30	-7.42E-01	-5.31E+02	16.00	-8.62E-01	-1.04E+02	132.00
p4	4	-9.82E-01	6.28E+02	2.62	-6.36E-01	-1.46E+02	41.40	-1.32E+00	6.32E+02	39.10	-5.12E-01	9.61E+02	28.60	-8.11E-01	1.30E+03	69.00	-1.06E+00	5.02E+03	440.00
p5	5	-7.56E-01	-9.08E+02	0.05	-5.25E-01	-2.03E+02	37.00	-7.11E-01	-5.93E+02	6.50	-7.43E-01	-2.23E+02	13.10	-6.66E-01	-5.66E+02	15.00	-5.88E-01	-1.32E+03	58.90
p6	6	-6.23E-01	-9.08E+02	0.05	-3.97E-01	-5.19E+02	12.60	-6.75E-01	-7.93E+02	1.16	-2.77E-01	-8.78E+00	15.90	-4.98E-01	-8.76E+02	6.00	-4.42E-01	-1.08E+03	73.10
p7	7	-6.97E-01	-9.08E+02	0.05	-5.32E-01	-6.08E+02	5.75	-1.16E+00	-8.03E+02	0.91	-9.53E-01	-2.76E+02	12.40	-1.08E+00	-1.05E+03	1.00	-9.07E-01	-2.12E+03	11.10
p8	8	-4.94E-01	-9.08E+02	0.05	-3.35E-01	-1.74E+02	39.30	-1.60E-01	-7.21E+02	3.09	-4.03E-01	-1.23E+02	14.40	-3.26E-01	-5.31E+02	16.00	3.42E-01	-2.29E+03	0.50
p9	9	-5.50E-01	-9.08E+02	0.05	-3.91E-01	-4.28E+02	19.60	-6.30E-01	-6.66E+02	4.55	-7.31E-01	-4.62E+02	9.96	-6.76E-01	-6.69E+02	12.00	-5.48E-01	-1.62E+03	40.80
p10	10	-5.63E-01	-9.08E+02	0.05	-5.60E-01	-6.67E+00	52.20	-4.66E-01	-5.26E+02	8.28	-7.84E-01	4.49E+02	21.90	-5.77E-01	8.90E+01	34.00	-8.26E-02	-1.23E+03	64.60
p11	11	-3.47E-01	-8.12E+02	0.21	-2.68E-01	-1.72E+02	39.40	-1.77E-01	-5.46E+02	7.74	-4.76E-01	1.97E+02	18.60	-2.86E-01	-1.52E+02	27.00	1.51E-01	-1.92E+03	22.80
p12	12	-3.22E-01	-5.73E+02	0.61	-4.47E-01	1.52E+02	64.50	-1.18E-01	-4.16E+02	11.20	-8.33E-01	2.81E+02	19.70	-5.39E-01	3.99E+02	43.00	-1.27E-01	-9.00E+02	84.20
p13	13	-1.85E-01	-9.08E+02	0.05	-1.66E-01	-2.51E+02	33.30	1.83E-01	-7.41E+02	2.54	9.76E-02	-1.69E+02	13.80	-7.45E-02	-5.66E+02	15.00	7.95E-01	-2.29E+03	0.50
p14	14	-1.01E-01	3.53E+02	2.16	-4.13E-01	4.34E+02	86.30	-1.35E-01	5.72E+01	23.80	-6.98E-01	4.47E+01	16.60	-5.84E-01	-1.52E+02	27.00	-6.05E-01	5.29E+02	170.00
p15	15	2.60E-02	-3.64E+02	0.96	-1.44E-01	1.34E+02	63.10	5.59E-01	-4.80E+01	21.00	5.37E-02	1.82E+02	18.40	2.89E-01	-1.87E+02	26.00	6.14E-01	2.46E+02	153.00
p16	16	6.32E-02	-9.08E+02	0.05	8.36E-02	-5.97E+02	6.60	6.08E-01	-8.22E+02	0.40	-2.01E-01	-1.11E+03	1.48	1.99E-01	-1.01E+03	2.00	-4.14E-02	-1.97E+03	19.80
p17	17	1.55E-01	-5.23E+00	1.56	-1.84E-01	6.12E+02	100.00	5.51E-01	2.31E+03	83.80	-3.32E-01	3.20E+02	20.20	4.25E-01	1.85E+03	85.00	-1.66E-02	3.14E+03	327.00
p18	18	5.24E-01	-6.57E+02	0.47	2.95E-01	-3.27E+02	27.40	8.68E-01	-4.54E+02	10.20	-2.49E-02	-5.42E+02	8.92	4.81E-01	-4.97E+02	17.00	5.47E-01	-9.93E+02	78.60
p19	19	7.51E-01	1.58E+03	4.22	2.82E-02	2.18E+02	69.60	5.94E-01	1.14E+03	52.60	9.17E-01	5.49E+02	23.20	6.70E-01	4.68E+02	45.00	9.79E-01	2.63E+03	296.00
p20	20	4.14E-01	2.92E+03	6.46	1.65E-02	3.70E+02	81.30	-3.05E-01	1.35E+03	58.30	-4.42E-01	4.27E+02	21.60	-7.44E-01	7.09E+02	52.00	-2.07E+00	2.41E+03	283.00
p21	21	1.23E+00	-5.13E+02	0.71	6.61E-01	5.41E+01	56.90	1.69E+00	-3.75E+02	12.30	1.51E+00	6.79E+02	24.90	1.57E+00	8.90E+01	34.00	2.59E+00	-1.06E+03	74.70
p22	22	1.79E+00	7.85E+01	1.70	1.76E+00	-3.33E+02	27.00	2.24E+00	5.98E+02	38.20	2.50E+00	-6.61E+02	7.36	2.11E+00	-4.28E+02	19.00	-1.88E-01	-8.21E+02	88.90
p23	23	3.37E+00	7.73E+03	14.50	-9.89E-01	1.70E+03	184.00	2.03E+00	3.52E+03	116.00	-7.43E-01	1.58E+03	36.70	2.74E+00	3.88E+03	144.00	2.03E+00	6.34E+03	519.00
p24	24	-1.26E+00	-9.08E+02	0.05	3.97E+00	-6.41E+02	3.20	-1.69E+00	-4.99E+02	9.00	2.12E+00	-1.12E+03	1.30	-1.41E+00	-7.38E+02	10.00	-1.09E+00	-2.11E+03	11.30

Source: Calculations made in TruVariogram software.

Table s.3. Calculated normalized variance values $v(j)_{Norm}$ and critical point evaluation for the Warta River, Poland, based on data reported by Jaskuła et al. (2021). A VCC_{Norm} of 0.204 was applied to the 2017 dataset. The evaluation comprises 144 parameter-point combinations (6 parameters × 24 sample collection stations) for 2017.

	Minigraph																		
	v(q)|h(q)|a(q)	*v(j)*	*h(q)*	*a(q)*	*v(j)*	*h(q)*	*a(q)*	*v(j)*	*h(q)*	*a(q)*	*v(j)*	*h(q)*	*a(q)*	*v(j)*	*h(q)*	*a(q)*	*v(j)*	*h(q)*	*a(q)*
Sample	**Distance**	**Cd**			**Cr**			**Cu**			**Ni**			**Pb**			**Zn**		
p1	1	-1.55E+00	3.07E+02	0.53	-5.96E-01	6.13E+03	152.00	-1.01E+00	-5.73E+03	36.98	-4.34E-01	-3.23E+03	16.80	-9.81E-01	-1.96E+04	106.00	-1.37E+00	-2.36E+03	234.00
p2	2	-9.26E-01	4.22E+02	0.47	-5.02E-01	-7.25E+02	0.78	-9.44E-01	2.01E+03	2.93	-3.20E-01	1.36E+03	0.77	-6.62E-01	2.85E+03	5.99	-1.25E+00	-1.44E+03	168.50
p3	3	-1.62E-01	1.26E+03	0.03	-4.89E-01	-4.77E+02	6.26	-7.87E-01	1.29E+03	6.12	-5.07E-01	-1.34E+02	5.99	-5.27E-01	2.78E+03	6.32	-1.15E+00	1.53E+02	55.79
p4	4	1.87E-01	-6.65E+02	1.04	-5.32E-01	3.75E+02	25.05	-7.06E-01	-1.88E+03	20.07	-6.30E-01	-3.19E+03	16.66	-7.21E-01	-5.16E+03	41.66	-1.03E+00	-1.99E+03	207.50
p5	5	2.97E-01	7.27E+02	0.31	-4.57E-01	-5.74E+02	4.12	-7.50E-01	-5.72E+02	14.30	-2.51E-01	6.61E+02	3.21	-7.58E-01	-2.07E+03	27.90	-7.41E-01	5.00E+02	31.20
p6	6	1.17E-01	9.94E+02	0.17	-4.62E-01	-4.63E+02	6.57	-4.86E-01	1.51E+03	5.12	-6.90E-01	-1.31E+03	10.11	-5.69E-01	2.79E+03	6.26	-7.73E-01	2.56E+02	48.48
p7	7	-1.10E-01	1.09E+03	0.12	-4.45E-01	-5.70E+02	4.20	-4.74E-01	1.66E+03	4.49	-5.17E-01	8.73E+02	2.47	-5.29E-01	3.45E+03	3.32	-6.64E-01	7.50E+02	13.52
p8	8	-3.06E-01	9.56E+02	0.19	-4.33E-01	-4.28E+02	7.33	-4.93E-01	9.78E+02	7.48	-4.37E-01	-2.03E+02	6.23	-4.42E-01	2.46E+03	7.72	-3.70E-01	5.19E+02	29.84
p9	9	9.54E-02	1.26E+03	0.03	-4.05E-01	-6.04E+02	3.46	-1.08E-01	2.36E+03	1.42	-6.63E-01	5.04E+02	3.76	-3.49E-01	3.77E+03	1.91	-5.25E-01	5.97E+02	24.31
p10	10	2.71E-01	1.26E+03	0.03	-3.65E-01	-6.29E+02	2.90	2.07E-01	2.13E+03	2.40	-2.28E-01	8.73E+02	2.47	-3.00E-01	3.72E+03	2.13	-7.55E-02	6.64E+02	19.62
p11	11	3.98E-01	1.20E+03	0.06	-3.39E-01	-6.04E+02	3.46	2.68E-01	1.82E+03	3.79	-1.36E-01	8.41E+02	2.58	-2.83E-01	3.22E+03	4.35	-2.42E-01	6.42E+02	21.11
p12	12	5.17E-01	7.27E+02	0.31	-3.70E-01	-1.36E+02	13.79	3.47E-01	1.11E+03	6.91	-3.72E-01	-2.40E+02	6.36	-2.19E-01	1.88E+03	10.30	2.82E-02	1.59E+02	55.35
p13	13	5.45E-01	2.88E+02	0.54	-2.59E-01	-6.97E+02	1.41	2.50E-01	1.02E+03	7.30	-1.22E-01	1.27E+03	1.09	-1.32E-01	3.53E+03	2.94	3.50E-01	8.55E+02	6.09
p14	14	9.38E-01	4.79E+02	0.44	-3.00E-01	-7.03E+01	15.23	4.28E-01	7.03E+02	8.69	-1.68E-02	4.69E+02	3.88	-9.07E-02	2.15E+03	9.12	4.72E-01	2.85E+02	46.45
p15	15	6.79E-01	7.65E+02	0.29	-2.19E-01	-4.38E+02	7.11	5.10E-01	1.88E+03	3.52	-4.73E-01	1.02E+03	1.94	-7.21E-03	2.64E+03	6.90	1.91E-01	5.78E+02	25.67
p16	16	7.09E-01	-8.75E+02	1.15	-1.42E-01	-6.17E+02	3.17	-2.73E-01	-3.11E+01	11.92	-5.54E-03	1.11E+03	1.65	1.20E-01	3.32E+03	3.90	5.99E-01	8.13E+02	9.05
p17	17	9.49E-01	1.22E+03	0.05	-7.67E-02	-5.49E+02	4.68	5.88E-01	1.58E+03	4.82	-2.93E-01	1.03E+03	1.93	1.94E-01	2.86E+03	5.95	-5.38E-01	7.37E+02	14.44
p18	18	1.84E+00	-2.50E+03	2.00	-1.32E-01	3.45E+02	24.40	4.52E-01	-2.85E+03	24.34	-8.60E-02	-5.63E+02	7.49	3.35E-01	-6.07E+02	21.38	6.06E-02	-4.31E+02	97.10
p19	19	1.61E+00	-4.84E+03	3.23	-1.50E-01	8.66E+02	35.89	6.24E-01	-2.27E+03	21.77	1.36E+00	-3.83E+02	6.86	5.04E-01	-6.09E+02	21.39	-1.15E-01	-4.10E+02	95.61
p20	20	1.58E-01	-5.39E+03	3.52	-1.83E-01	1.06E+03	40.26	-2.25E+00	-6.19E+03	39.00	-7.83E-01	-3.17E+03	16.60	6.22E-02	-2.95E+03	31.81	-2.70E-01	-1.51E+03	173.50
p21	21	-1.26E+00	4.05E+01	0.67	4.31E-01	-2.77E+02	10.66	-7.35E-02	3.67E+02	10.17	7.70E-01	2.69E+02	4.58	5.94E-01	1.91E+03	10.18	1.87E+00	3.94E+02	38.67
p22	22	-1.66E+00	1.09E+03	0.12	1.02E+00	-6.65E+02	2.12	9.75E-01	4.96E+02	9.60	1.08E+00	1.42E+03	0.56	2.37E+00	3.27E+03	4.12	2.10E+00	6.72E+02	19.02
p23	23	-1.61E+00	-9.13E+02	1.17	1.23E+00	2.06E+02	21.33	4.32E-01	-9.84E+02	16.11	-2.26E-01	-3.11E+02	6.61	3.41E+00	5.52E+02	16.22	1.42E+00	-1.92E+01	67.95
p24	24	-1.72E+00	1.09E+03	0.12	4.18E+00	-4.63E+02	6.56	3.27E+00	-4.02E+02	13.55	3.97E+00	1.03E+03	1.91	-1.02E+00	-1.61E+04	90.47	2.02E+00	-4.08E+02	95.45

Source: Calculations made in TruVariogram software.

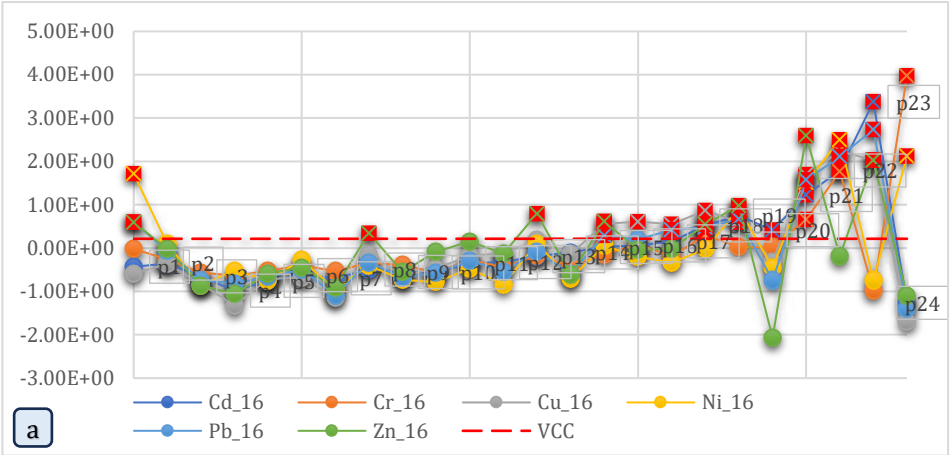

(a) Composite variogram for the year 2016.

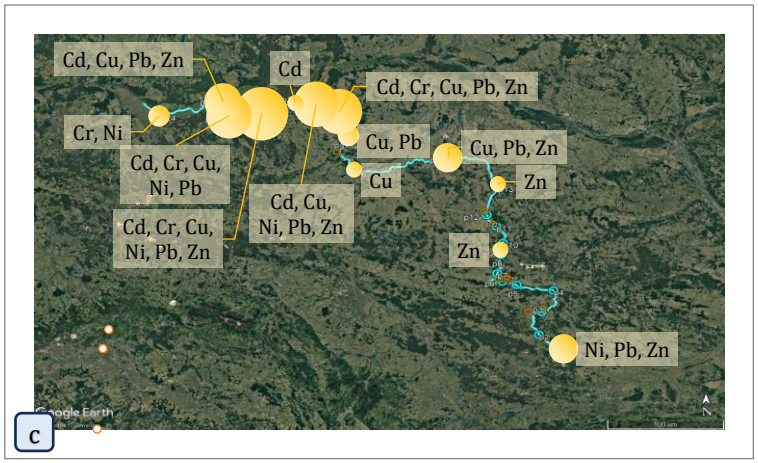

(c) Map of critical point evaluation for the year 2016.

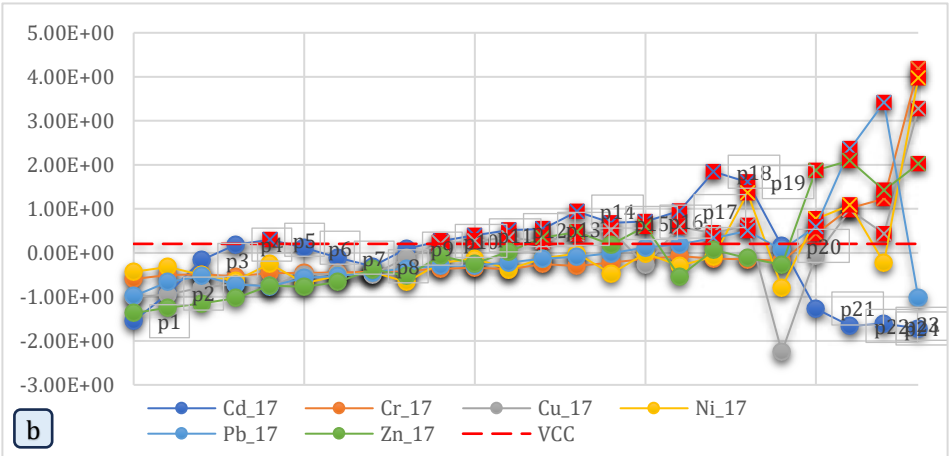

(b) Composite variogram for the year 2017.

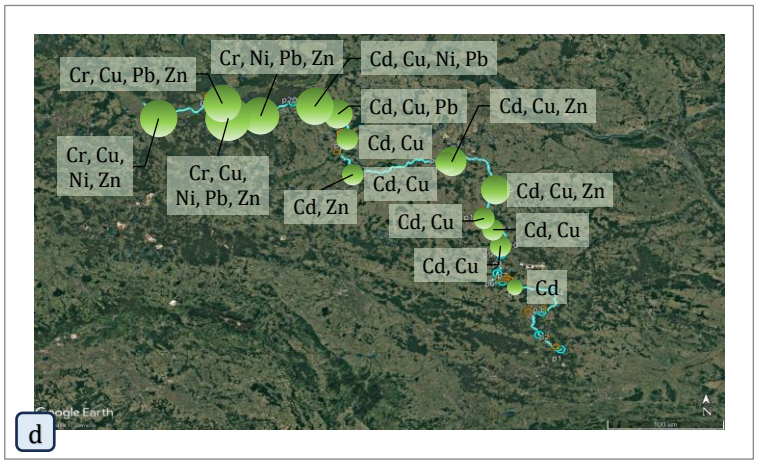

(d) Map of critical point evaluation for the year 2017.

In both variograms, the x-axis labels from p1 to p24 indicate the sampling station associated with each normalized variance value $v(j)_{Norm}$ via the relationship $v(q) = v(j-1)$ (Equation 14). Red squares marked with an "X" indicate values exceeding the defined VCC_{Norm}.

Figure s.1. Composite normalized variograms and maps highlighting critical points derived from the study by Joanna Jaskuła et al. (2021) on the Warta River, Poland. A normalized VCC_{Norm}) of 0.215 was applied to the 2016 dataset and 0.204 to the 2017 dataset.

Source: Authors' own elaboration based on TruVariogram software. Satellite images from Google Earth, 2025.

Table s.4. Normalized variance values $v(j)_{Norm}$ and critical point evaluation for the Elbe River, Germany, based on data reported by (Brack et al., 2008). A VCC_{Norm} of 0.173 was applied to the TOC-normalized composite variogram. The evaluation comprises 27 parameter-site combinations (3 parameters × 9 sampling stations, TOC basis).

	Minigraph											Global: 27	14
	v(j)|h(q)|a(q)	*v(j)*	*h(q)*	*a(q)*	*v(j)*	*h(q)*	*a(q)*	*v(j)*	*h(q)*	*a(q)*			*51.9%*
Sample	**Distance**	**PCB**			**PCDD**			**PCNs**			**A: Param.**	**B: Cnt.**	**C: %**
KON	1	-1.47E+00	-1.34E+02	8.34	-6.97E-01	1.56E+01	23.33	-1.29E+00	1.41E+01	21.67			
DRE	2	-3.30E-01	-2.00E+00	21.24	1.29E-01	1.91E+01	38.42	4.12E-02	2.91E+01	2.63			
TOR	3	6.31E-01	1.35E+02	34.54	5.76E-01	1.54E+01	29.71	1.02E+00	1.50E+01	19.81	PCB, PCDD, PCNs	3	100.00%
WIT	4	3.34E-02	1.01E+02	29.31	3.58E-01	2.00E+01	4.73	5.47E-01	2.80E+01	4.43	PCDD, PCNs	2	66.70%
LEO	5	5.88E-01	-1.40E+00	21.26	5.61E-01	-1.03E+01	1133.70	4.34E-01	3.47E+00	43.62	PCB, PCDD, PCNs	3	100.00%
BAR	6	1.49E+00	8.72E+01	28.20	7.73E-01	-1.51E+01	1210.85	9.51E-01	-4.50E+01	125.16	PCB, PCDD, PCNs	3	100.00%
MAG	7	-2.51E-01	-5.36E+01	16.17	1.29E+00	-7.69E+01	3993.56	8.36E-01	-9.42E+01	245.53	PCDD, PCNs	2	66.70%
ARN	8	-1.45E+00	-1.44E+02	10.14	-1.50E+00	1.84E+01	61.30	-1.26E+00	3.02E+01	0.87			
HIT	9	7.61E-01	1.17E+01	22.54	-1.49E+00	1.38E+01	101.93	-1.28E+00	1.93E+01	10.95	PCB	1	33.30%

Source: Calculations made in TruVariogram software.

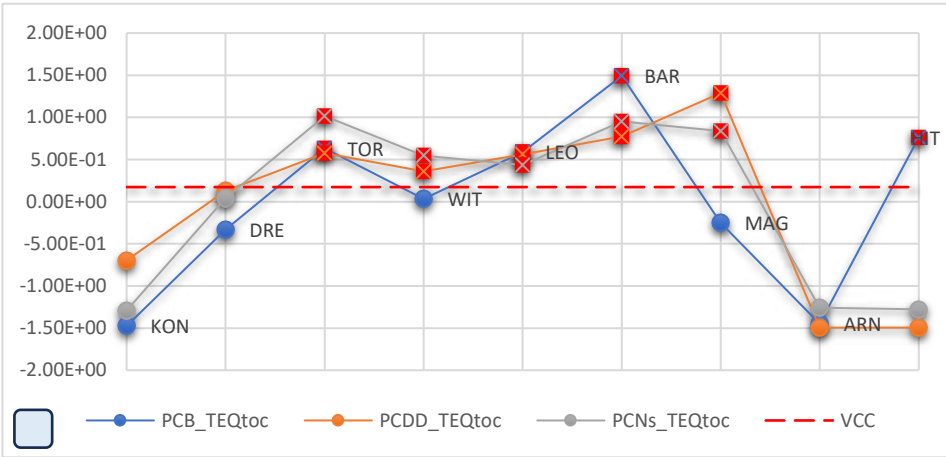

(a) Composite normalized variogram (TOC basis).

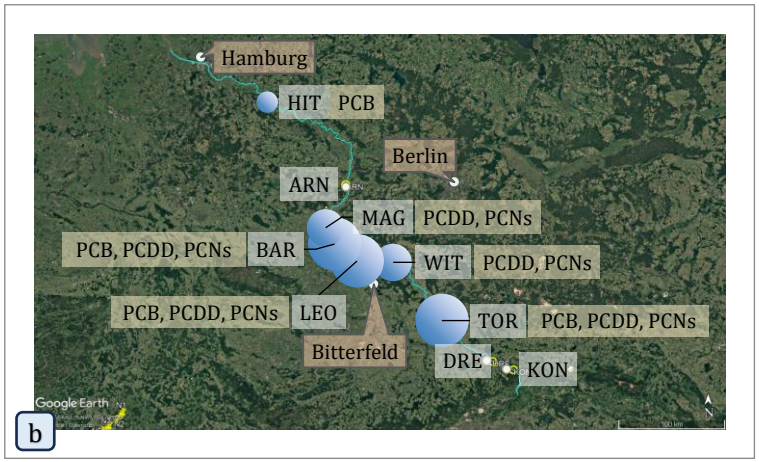

(d) Map of critical point evaluation.

In the variogram, the x-axis labels indicate the sampling station associated with each normalized variance value $v(j)_{Norm}$ via $v(q) = v(j-1)$ (Equation 14). Red squares marked with an "X" indicate values exceeding the defined VCC_{Norm}.

Figure s.2. Composite normalized variogram and map highlighting critical points derived from the study by (Brack et al., 2008) on the Elbe River, Germany. A VCC_{Norm} of 0.173 was applied to the TOC-normalized dataset.

Source: Authors' own elaboration based on TruVariogram software. Satellite images from Google Earth, 2025.

TruVariogram: A VBA-Excel™ application for one-dimensional heterogeneity variography and VCC_{Norm}-based critical point identification

Software and Data Availability

- Name of software: TruVariogram
- Developers: Christian Romero Prieto
- Contact: ductor@nostertec.com
- Date first available: April 8, 2025
- Software required: Excel™ 2016 (365 preferred)
- Program language: VBA-Excel
- Source code at: https://github.com/chemistCARP/TruVariogram
- Documentation: Detailed documentation for application, testing, and deployment can be found at https://github.com/chemistCARP/TruVariogram/blob/main/README.md
- Data required for local installation and use of software is accessed through the cloud. See Data Availability Statement.

TruVariogram is a VBA-Excel™ application developed by the author of this publication as part of work conducted at Noster Tec. The tool performs variographic analyses by automatically generating individual spreadsheets for environmental parameters measured at sampling points arranged in a one-dimensional ordered sequence. Although the methodology is most naturally applied to river monitoring transects, it is equally applicable to soil profiles, geological boreholes, vertical well sampling, lake or marine transects, and time-series measurements at fixed stations — any context in which samples can be arranged in a defined linear order. This includes fixed-location temporal monitoring in the mining-metallurgical industry and stationary watercourse stations where samples are collected at regular intervals.

Key Features of TruVariogram

- **Critical points and parameters**: Identifies and assesses critical sampling points and parameters using heterogeneity variography and the VCC or VCC_{Norm} criterion (Equation 7).
- **Critical points and parameters**: Identifies and assesses critical points and parameters using variography and the VCC methodology.
- **Automated spreadsheets**: Generates individual spreadsheets for each environmental parameter measured at sampling points along a one-dimensional system.
- **Variogram creation**: Automatically produces normalized composite variograms and provides evaluation tools to compare $v(j)_{Norm}$ values against the estimated VCC_{Norm}.
- **Variogram creation**: Automatically produces variograms and provides evaluation tools to compare values against VCC, as detailed in this document.
- **Sampling prediction**: Enables users to estimate the required number of sampling points based on the desired or achievable sampling error for each variogram constructed.
- **Physical space conversion**: Converts statistical variogram spaces into physical spaces, presenting results clearly in tables and charts.
- **Combined variograms**: Introduces an innovative concept of combined variograms, allowing users to create a single chart displaying multiple selected variograms.
- **Data cloning**: Supports parallel evaluations by duplicating datasets.
- **Map-integrated results**: Introduces a novel Excel™ chart type, "ChartMap," which integrates sampling point maps (e.g., those created in Google Earth™) with VCC evaluation results. Sampling point coordinates are required to depict critical points and parameters such as labels or circles sized proportionally to environmental impact.
- **Multiple coordinate systems**: Supports five coordinate types and includes positioning calibration tools.
- **Spreadsheet Organization Tools**: Offers features to organize spreadsheets with color-coding and standardized naming conventions for enhanced usability.

Concise overview of the TruVariogram environment and its basic usage

In the "Model" worksheet, click the button 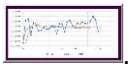 . This will display a floating toolbar, as shown in Figure s.3. Manually, users can duplicate the worksheet named "Model," rename it, and enter data into the cells under the light blue columns (see Figure s.4.a). After inputting the sample identification, mass (or volume), and parameter concentration, clicking the beaker icon button will trigger TruVariogram to perform calculations and display the results in variography charts. If mass or volume data for the samples are unavailable, users can enter an arbitrary value for all samples (e.g., 1.00), except for at least one sample, which must have a slight difference (e.g., 1.01). This is necessary because, during mass (or volume) normalization, the standard deviation must be non-zero (see Equation 11).

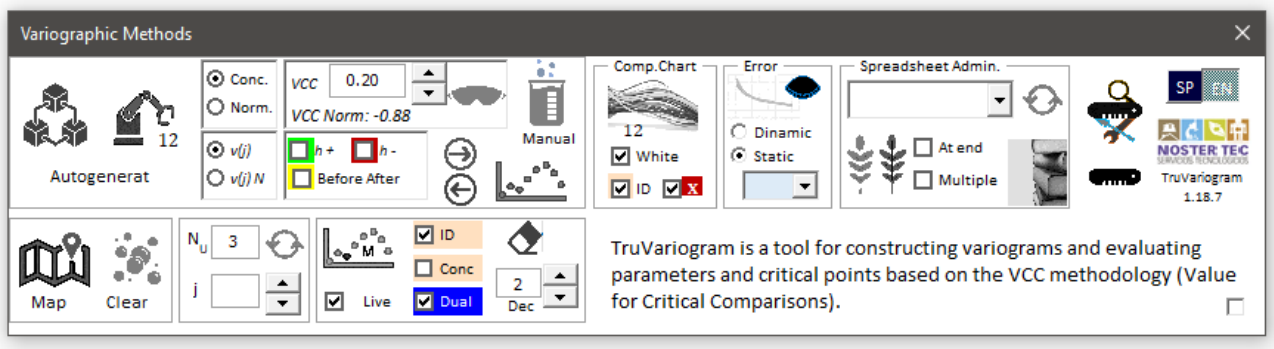

Figure s.3. TruVariogram environment showing the main toolbar (floating), the VCC_{Norm} configuration field, and additional tools including the composite variogram and ChartMap panels.

Source: TruVariogram version 1.18.7

n	Sample ID	Distance	m_q, [g]
1	VR	1	1.01
2	OR1	2	1
3	23P	3	

a

Mass/Vol	Sample	COD	As	Ca	Cr
1.00	VR	4050.845	91.050	8779.735	90.830
0.95	OR1	1639.375	34.485	1418.555	113.290
1.50	23P	1151.370	37.350	2089.715	91.005
1.20	UZT2	1150.190	31.385	2337.335	[illegible]

b

Figure s.4. (a) Fields to be manually completed by the user.
(b) Example table with data for declaration in automatic mode.

Source: TruVariogram version 1.18.7

For greater convenience, an automated method allows users to create entire batches and their corresponding variograms. To do so, in a calculation worksheet, users must have data on sampling points, masses (or volumes), and parameter results, as shown in Figure s.4.b. The automatic functions of TruVariogram are described below:

The tool prompts the user to select the cell range containing sample names, followed by the range for masses (or volumes), and finally, the complete range of measured parameters. It automatically creates a worksheet for each parameter.

A new window appears, dynamically generated based on the number of parameters, with each column accommodating up to 12 parameters by default. After selecting the parameters, variogram construction begins according to the methodology and criteria outlined in this document. A criteria configuration panel is displayed here on the right.

Another dynamically generated window allows users to optionally specify the name of the new worksheet. Once the parameters to combine are selected, a new worksheet is created, containing the criteria, variance (as explained in the methodology), heterogeneity, and parameter values.

Mini-charts are included, and values exceeding the VCC_{Norm} or configured optional criteria are highlighted in red. A partial screenshot of this is shown below:

	Conc.	*			*		
	Conc.Norm.						
	VCC	0.2			0.2		
	VCC Norm.						
	Before After						
	Heterogeneity (+)(-)						
	Sparkline						
	v(j)|h(q)|a(q)	*v(j)*	*h(q)*	*a(q)*	*v(j)*	*h(q)*	
Sample	**Distance**	**PCB_dw**			**PCB_toc**		
KON	1	7.37E-02	-9.12E-01	0.10	0.00E+00	-6.06E-01	
DRE	2	9.89E-02	-2.54E-01	0.89	1.13E-01	-3.23E-03	
TOR	3	2.43E-01	2.00E-01	1.43	2.07E-01	6.18E-01	...

	Ref.1				Global	35		
a(q)	*Ref.2*					*64.8%*		
	Muestra	**Lat**	**Lon**	**A: Param.**	**B: Cnt.**	**C: %**	**D: [ ]**	
21.67	KON			PCDD_Fs_dw	3	50.00%		
2.63	DRE			PCDD_Fs_dw	4	66.70%		
19.81	TOR			PCB_dw, PCE	6	100.00%		
...								

TruVariogram includes a dedicated toolbar for creating ChartMaps —a novel Excel™ chart type that overlays georeferenced sampling point data onto satellite or field maps, displaying critical parameters as labeled circles sized proportionally to the percentage of critical parameters at each station. Its primary functions are outlined below.

From the combined variograms worksheet, clicking the map icon button or the "Map Tools" button will display a toolbar (see Figure s.5). Accepted geographic position data are latitudes and longitudes expressed as decimal numbers. Creating a map involves the following steps:

1. Insert a map using the globe-map icon button. Users will be prompted to upload a map (e.g., from geographic software like Google Earth™). The map must include markers for sampling points and, crucially, two reference points at opposite diagonal corners of the map.
2. Click the "pin 1" icon and indicate the cell containing the latitude of the first reference coordinate, followed by the cell with its longitude. TruVariogram allocates a space for reference and sample coordinates, located to the right of the combined data (scroll right to view).
3. Repeat the process for "pin 2" to input the second reference coordinate.
4. Click the "compass" icon to select the range containing the latitudes and longitudes of the samples (headers are not required).
5. Click the "map sheet" (place) icon to plot the points on the map. If point visibility is suboptimal, choose a different color and re-place the points. The spin buttons 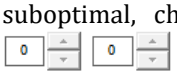 will help fine-tune point placement on the ChartMap. If the scale appears distorted, select a different projection (Mercator is the default). However, changing projections requires re-entering both reference points, so repeat from step 2.
6. Check the "Multiple" box to generate multiple layers on the ChartMap:
   a. Click "Label." Column [A] contains identified critical parameters; [B] indicates the count of critical parameters; [C] represents the percentage of critical parameters relative to the total parameters per sampling point; and [D] is a user-defined column for additional data.
   b. Click the compass icon to specify the range of latitudes and longitudes for the new ChartMap layer.
   c. Click the map (multi-place) to display labels on the ChartMap.

Note 1: Circle sizes on the ChartMap can be adjusted using the spin buttons 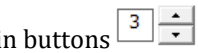

.

Note 2: Selecting "C" in the Label box activates the "Auto Size" option, where users can set a value (default is 15) for circle sizes proportional to the percentage of critical parameters per sampling point.

Note 3: Different colors can be selected for each layer by using

.

Note 4: Manual labels can be added. Enter the label content, select a point on the ChartMap, and click the "speech bubble" icon:
.

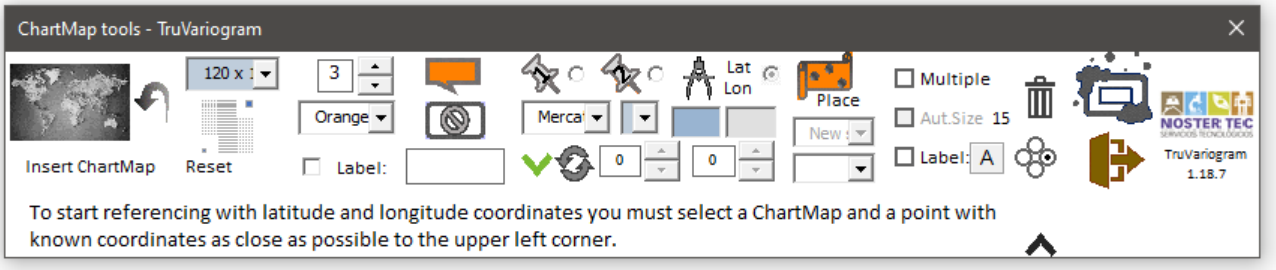

Figure s.5. ChartMap Creation Environment in TruVariogram. The complete interface is shown, including additional tools and a dialog box (bottom left).

Source: TruVariogram version 1.18.7